ABSTRACT

Title of Document: AN ACTIVE NON-INTRUSIVE SYSTEM IDENTIFICATION APPROACH FOR CARDIOVASCULAR HEALTH MONITORING

Nima Fazeli, Master of Science, 2014

Directed By: Professor Jin-Oh Hahn, Department of Mechanical Engineering

In this study a novel active non-intrusive system identification paradigm is developed for the purpose of cardiovascular health monitoring. The proposed approach seeks to utilize a collocated actuator sensor unit devised from the common blood pressure cuff to simultaneously 1) produce rich transmural blood pressure waves that propagate through the cardiovascular system and 2) to make measurements of these rich peripheral transmural blood pressures utilizing the pressure oscillations produced within the cuffs bladder in order to reproduce the central aortic blood pressure accurately. To achieve this end a mathematical model of the cardiovascular system is developed to model the wave propagation dynamics of the external (excitation applied by the cuff) and internal (excitation produced by the heart) blood pressure waveforms through the cardiovascular system. Next a system identification protocol is developed in which rich transmural blood pressures are recorded and used to identify the parameters characterizing the model. The peripheral blood pressures are used in tandem with the characterized model to reconstruct the central aortic blood pressure waveform. The results of this study indicate the developed protocol can reliably and accurately reproduced the central aortic blood pressure and that it can outperform its intrusive passive counterpart (the Individualized Transfer Function methodology). The root-mean-square error in waveform reproduction, pulse pressure error and systolic pressure errors were evaluated to be 3.31 mmHg, 1.36 mmHg and 0.06 mmHg respectively for the active nonintrusive methodology while for the passive intrusive counterpart the same errors were evaluated to be 4.12 mmHg, 1.59 mmHg and 2.67 mmHg indicating the superiority of the proposed approach.

AN ACTIVE NON-INTRUSIVE SYSTEM IDENTIFICATION APPROACH FOR CARDIOVASCULAR HEALTH MONITORING

By

Nima Fazeli

Thesis submitted to the Faculty of the Graduate School of the
University of Maryland, College Park, in partial fulfillment
of the requirements for the degree of
Master of Science
2014

Advisory Committee:
Professor Jin-Oh Hahn, Chair
Professor Balakumar Balachandran
Professor Nikhil Chopra

Table of Contents

List of Tables

List of Figures

Chapter 1 - Importance of Cardiovascular Disease Diagnosis and Prevention

1.1: Importance of Cardiovascular Disease in Modern Day Society

Cardiovascular Disease (CVD) is one of the most prevalent sources of morbidity and mortality in modern times. The World Health Organization estimates that CVD is responsible for approximate 1 in 3 deaths worldwide [1] and billions of dollars are spent in direct costs [2]. The American Heart Association (AHA) [3] reports that CVDs are responsible for 1 in every 3 deaths (32.8%) in the United States (which is approximately 1 death every 39 seconds) and that CVDs have extremely high impacts on society in general. During the decade between 1999 and 2009 the number of procedures associated with CVDs has increased by 22% and indicates a growing and ever more prevalent problem. In addition to this increase in the number of CVD, the healthcare cost associated with this category of diseases is higher than any other diagnostics group which compounds the problem of treatment and increases burden on resources available. Prevention of CVDs, including early identification and treatment, can save billions, for example the healthcare cost of CVDs, strokes and related conditions was approximately $300 billion dollars, compared to the $228 billion associated with cancers.

Hypertension, a very common type of CVD, is defined as a patient having systolic blood pressure of above 140 mmHg and/or diastolic blood pressure above 90 mmHg. Hypertension is well-known and widely accepted as a risk factor of CVDs [4] and astonishingly approximately 76,400,000 out of approximately 82,600,000 adult Americans having CVDs suffer from hypertension. Of these hypertensive individuals approximately 4 out of 5 are aware of the fact that they suffer from hypertension and 1 in 5 do not even have knowledge of this very important risk factor. Of these individuals 75% are under current treatment, but unfortunately, only 53% have it controlled with the remaining 47% having it uncontrolled [3]. In addition, hypertension is much more prevalent in the elderly population (more than 50% in individuals with age>55, which further complicates and emphasizes the seriousness of CVD since the older population has higher chances of having other health problems in addition to CVD. Further, the rate of death from hypertension as well as the actual number of deaths is estimated to have been increasing, with the resulting healthcare cost of ~$51 billion in 2009. Considering the tremendous impact of CVD on the quality of life, it is imperative to develop a systematic method that is readily accessible to assess hypertension and CVD to closely monitor CV health, promptly detect CVD, and effectively manage CVD risk factors and parameters.

1.2: Techniques for Monitoring of Cardiovascular Health: State of the Art and Shortcomings

Blood pressure in the arterial tree is produced by the pressure differential across the left ventricle of the heart. Blood pressure waveforms are lateral waveforms that propagate along the arterial pathways in the body and also undergo multiple reflections. To better understand the wave propagation dynamics typically the wave ejected by the heart is treated as the forward traveling wave and the reflected waveforms from the peripheries is treated as the backward traveling wave [5]. The superposition of these two waveforms creates the waveform that is seen at every point along the propagation pathway. The waveform morphology itself changes along the propagation pathway typically increasing in systolic blood pressure (highest pressure achieved by) while small drops in diastolic (lower blood pressure) and mean blood pressure are observed [6].

Due to its proximity to the heart, it is central aortic BP that is more informative about cardiac dynamics and global circulation and thus provides greater clinical value than those measured in the periphery. Indeed, it is increasingly accepted that central hemodynamic measurements can enhance CV risk prediction [7], as well as reflect changes in the arterial tree that is independent of brachial BP levels [8] [9]. Due to this importance of central aortic BP high-fidelity, point-of-care non-invasive measurement of central aortic hemodynamics is important for clinical CV health monitoring and risk assessment. In fact, clinical research supports the central aortic measurements such as central aortic BP, augmentation index, reflection magnitude and index as well as pulse wave velocity as significant predictors of CV risk.

1. Central Aortic BP:
   As already mentioned this parameter is very important in both health and disease [10],[11],[12], and accurate measurement of this parameter is a useful tool for the assessment of the overall CV risk [13], [14].
2. Augmentation Index:
   Augmentation index is defined as the ratio of augmented BP over central pulse pressure measured at the central aorta and is an indicator of arterial stiffness, wave reflection and loads imposed on the heart by the arterial tree. The increase of this parameter has been shown to correlate with an increase in CV risk [15], [16].
3. Reflection Magnitude and Index:
   This parameter is an indicator of relative magnitude of the backward traveling wave when compared to the forward traveling wave and is important because early wave reflection is associated with increase in load of the heart [17], [18].
4. Pulse Wave Velocity:

Pulse Wave Velocity (PWV) is the speed at which the arterial BP waveform propagates through the arterial pathway and is used as a surrogate measure of arterial stiffness [15],[19].

Ideally speaking the measurement and interpretation of the CV risk factors must low-cost, easy to access, easy to use, be taken noninvasively as well as accurately and finally must be patient specific. To date the existing and state-of-art methods cannot satisfy all the constraints and each method has a significant shortcoming. Measurement of the central aortic BP is typically done with aortic catherization which is an invasive, costly, risky and uncomfortable procedure. A common noninvasive replacement is carotid artery applanation tonometery but while this technique is noninvasive it requires significant expertise and training to be done correctly and carotid artery BP is not always a sufficiently accurate estimate of central aortic BP [20]. A potential replacement may be peripheral blood pressure measurements, these measurements can be made noninvasively but several fundamental flaws exist in this approach that does not make it a suitable replacement to central aortic BP. Peripheral blood pressure measurements as mentioned previously differ in morphology to central aortic blood pressure measurements due to wave reflection phenomena and also the devices that seek to measure peripheral BP waveforms are typically expensive [21]. The Generalize Transfer Function methodology has been developed to estimate central aortic blood pressure from peripheral measurements but this technique is not patient specific and so cannot always provide an accurate or reliable estimation of central blood pressure [38]. Furthermore, other methods to infer the central aortic blood pressure from peripheral blood pressure measurements using population averaged models has previously been proposed [22] and [23]. Though these methods do give estimates of the central aortic blood pressure they are not subject specific and are not tailored to each individual case and are often skewed towards the physiology of subjects that the population averages have been taken over and so may not necessarily be representative of more diverse subject pools.

1.3: Thesis Objective and Outline

The goal of this thesis is to develop an innovative low-cost and non-invasive method for monitoring of CV health and CVD, which can infer subject-specific central aortic blood pressure which can be used to evaluate CV risk factors. The method consists of a low-cost and non-invasive modality for measuring arterial circulatory waveforms at the body's extremity locations (such as peripheral BP waveforms, e.g., at radial and femoral arteries; note that peripheral measurements are easier to obtain compared with their central aortic counterparts) and an adaptive, subject-specific algorithm for

estimating central aortic CV parameters (i.e., risk factors) from the measured peripheral circulatory waveforms. In the proposed framework, CV risk factors are derived in 3 steps. First, two peripheral circulatory waveform signals are measured at the body's diametric locations of an individual (Step 1; note that central aortic signals not amenable to measurement are not involved). Second, the CV dynamics of the individual is characterized based on an adaptive signal processing algorithm that fits a CV model to the measured circulatory waveforms (Step 2; note that the resulting CV model can provide subject-specific CV parameters such as PWV, since it is fitted to a specific individual). Third, central aortic BP waveform is estimated by de-convolving the peripheral circulatory waveforms from the characterized CV model (Step 3; note that AI is also derived from the estimated central aortic BP in this step).

There are a number of key advantages in the proposed method compared with the traditional methods described in the previous section: (i) the method can be implemented to be of low cost and non-invasive via appropriate choice of the measurement modality; (ii) it can eliminate the use of central aortic measurements; and (iii) it provides CV parameters and risk factors that are specific to individual subject, thereby enabling subject-specific monitoring of CV health and CVD. In this regard, the proposed system has potential to meet all the aforementioned specifications of a medical system for CV health monitoring that is readily accessible to the general public to make real impact: low-cost, easy and non-invasive as well as accurate and reliable, and most importantly, subject-specific.

In chapter 2 the tube-load model which is the basis of the proposed methodology is introduced and validated in humans. In chapter 3 the "Individualized Transfer Function" (ITF) methodology is introduced which uses peripheral blood pressures measured invasively to estimate central aortic blood pressure. The ITF methodology will be validated in humans using experimental data and will serve as a special case of the proposed methodology. In chapter 4 the "Active Noninvasive Cardiovascular System Identification" methodology will be introduced and discussed at length, the purpose of this methodology is to overcome the shortcomings of the ITF methodology by developing a framework to make noninvasive accurate peripheral blood pressure measurements and also to alleviate the issue of lack of persistent excitation in the signals produced by the heart. The framework is implemented with an amalgamation of experimental and synthetic data to demonstrate the feasibility of the approach.

Chapter 2 - Validation of the Tube-Load Model in Humans

2.1: Introduction to the Tube-Load Model and Cardiovascular Health Monitoring

Substantial research effort has been put into the development of models in order to better understanding the cardiovascular system physiology and to develop techniques applicable to monitoring of arterial hemodynamic. The models developed can be classified into two categories: lumped parameter models and distributed parameter models. Lumped parameter models are structurally quite simple and are characterized by a small number of parameters which can be easily estimated from arterial waveforms available in clinical practice. Perhaps the most prevalent lumped parameter model is the Windkessel model [24]. Windkessel is a German word often loosely translated to chamber of air and in its simplest form is characterized by 2 parameters, R and C and is depicted in Figure 2-1. As can be seen the Total Peripheral Resistance (TPR) of the arterial tree is modeled using a resistor (R) and the arterial compliance of the cardiovascular system is modeled using a capacitor (C).

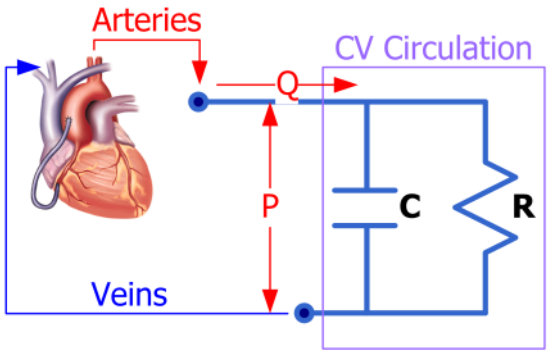

Figure 2-1: Simple Windkessel Model

Although estimation and interpretation of the model parameters in lumped models are generally simple, these models inherently assume an infinite Pulse Wave Velocity (PWV) and suffer from the inability to reproduce wave reflection or propagation phenomena which are key in arterial waveform construction. In contrast to lumped parameter models, distributed parameter models are capable of describing wave propagation and reflection dynamics by allowing for finite PWV [25, 26]. Many distributed parameter models utilize simplified Navier-Stokes equations regarding fluid dynamics to describe wave propagation dynamics and are characterized by parameters that describe geometry and mechanical properties of the arteries, such studies include Wang et al. [27], Burattini et al. [28] and Campbell et al. [29]. Though these models tend to offer much more accurate reproduction of arterial hemodynamics, they are typically mathematically cumbersome and in practice prove

to be very difficult to identify reliably due to the excessively large number of parameters involved in their structure and this major limitation has inhibited their application in clinical practice.

A middle ground model structure dubbed the tube-load model has undergone much investigation due to its ability to describe wave propagation and reflection dynamics while simultaneously being mathematically tractable and characterisable by a small number of parameters. As this class of model has gained popularity it has been used in the estimate of important clinical hemodynamic measures such as cardiac output (CO) in studies such as Welkowitz et al. [30], aortic blood pressure (BP) and flow (BF) waveform in studies such as Karamanoglu et al. [22]. Most existing efforts have aimed to reconstruct or infer information about the central aortic blood pressure due to the importance of this measure in clinical practice.

Due to the potential applicability of these models in clinical settings, substantial effort has been put into the validation of the tube-load models, though the vast majority of research efforts have been geared towards the validation of these models in animals. Table 2-1 depicts research efforts geared towards the validation of the tube-load model in living beings.

Table 2-1 Studies of the Validation of Tube-Load Model

Year	Lead Author	Species
1989	Burattini [28]	Canine
1990	Campbell [29]	Canine
1993	Berger [31]	Canine
1995	Shroff [32]	Canine
1997	Fogliardi [33]	Canine
2000	Segers [34]	Canine
2009	Hahn [25]	Swine
2010	Xu [35]	Canine

There have only been a hand full of instances of the application of the tube-load in humans and even fewer studies attempting to quantitatively validate these models in humans. The primary reason why such few studies exist in humans is due to fact that arterial blood pressure measurements are difficult to accomplish at multiple points simultaneously, especially if one of these blood pressures is estimated at or close to the left ventricle of the heart. It is important to note that even with the existence of the difficulty of such measurements; establishing the validity of tube-load models in humans will provide a strong basis to extend the applicability of ongoing advances in novel cardiovascular monitoring method ([25], [32], [36] and so on) in humans.

In this chapter the contribution of this thesis related to the validation of the tube-load model in humans is discussed. In order to achieve this end the tube-load model is discussed in detail and a mathematical treatment of the identifiability and validation of tube-load model in humans is provided using clinical data measured from humans undergoing cardiopulmonary bypass. It is noted that the material in this chapter was presented by the author in [62].

2.2: Tube-Load Model Mathematical Formulation

Due to the importance of the tube-load model as a basis to many novel cardiovascular monitoring methods and it's potential as a highly prevalent model of the human hemodynamics, a through mathematical treatment as well analysis of structural identifiability are a necessary prerequisite to validation of the model in humans using experimental data. The tube-load model is a concept taken from transmission line theory and consists of a conduit (tube) ending with a load and being driven by some source, and in this study 2 tube-load models are analyzed, the 1 tube-load model and the 2 tube load model. The 1 tube-load model considered in this thesis is comprised of a lossless tube ending in a Windkessel load.

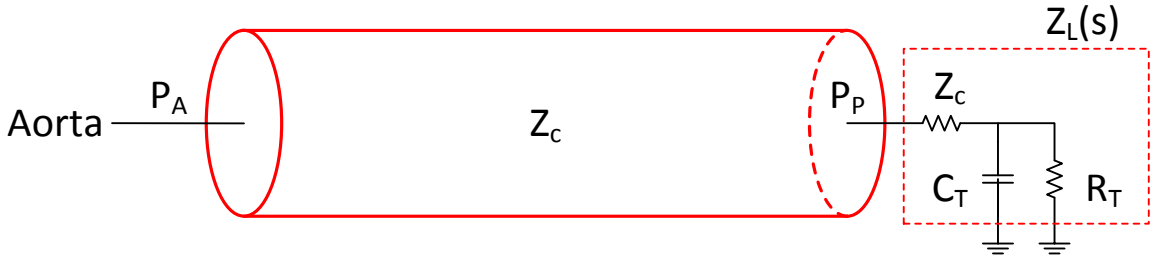

Figure 2-2 Tube-Load Model - Lossless Conduit Terminating with a Windkessel Load

Figure 2-2 depicts the considered 1 tube-load model, where Z_c denotes the conduit characteristic impedance, C_T represents the distal arterial compliance, R_T denotes the peripheral resistance and Z_L denotes the load impedance. The load impedance can be calculated as below:

$$Z_L = Z_c + \frac{R_T}{R_T C_T s + 1} \tag{1}$$

Where s denotes the Laplace frequency domain variable. It is important to note that at high frequencies the load impedance approaches the characteristic impedance, this means that high frequency waves do not undergo any reflection at the load site and are absorbed by the load, this is a critical characteristic of physiological

cardiovascular systems [29]. The transfer function relating central aortic blood pressure (P_A) to peripheral blood pressure (P_P) is given by:

$$P_P(s) = G(s)P_A(s) = \frac{1 + \Gamma(s)}{e^{\tau s} + e^{-\tau s}\Gamma(s)} P_A(s) \tag{2}$$

Where τ denotes the Pulse Transit Time (PTT) which is the time required for the wave to propagate from one end of the tube to the other end and $\Gamma(s)$ denotes the reflection coefficient defined by Equation (3):

$$\Gamma(s) = \frac{Z_L(s) - Z_c}{Z_L(s) + Z_c} \tag{3}$$

Replacing $Z_L(s)$ into Equation (3):

$$\Gamma(s) = \frac{R_T}{2Z_c R_T C_T s + (2Z_c + R_T)} = \frac{\eta_2}{s + \eta_1} \tag{4}$$

Where $\eta_1 = \frac{2Z_c + R_T}{2Z_c R_T C_T}$ and $\eta_2 = \frac{R_T}{2Z_c R_T C_T}$, now replacing the η_1 and η_2 expressions into Equation (2):

$$P_P(s) = G(s)P_a(s) = \frac{s + \eta_1 + \eta_2}{(s + \eta_1)e^{\tau s} + \eta_2 e^{-\tau s}} P_A(s) \tag{5}$$

It is shown that the transfer function relating central and peripheral blood pressures is characterized by 3 parameters, the PTT and 2 polynomial coefficients.

The 2 tube-load model is comprised of two tubes with a resistor between the tubes (Figure 2-3). The resistor between the 2 tubes represents the blood flow loses due to bifurcations (for example the bifurcation of the brachial at the elbow into the radial/ulnar or the bifurcation of the descending aorta to the abdominal and femoral arteries) and splanchnic organs.

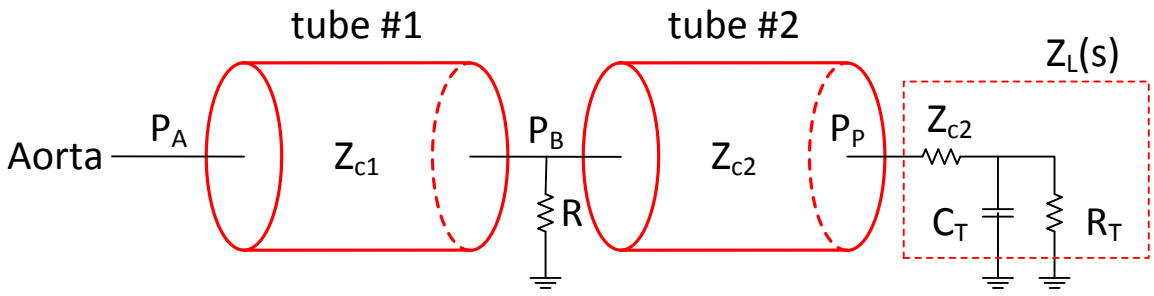

Figure 2-3 2 Tube-Load Model

Referring to Figure 2-3 the relationship between P_A and P_B is given by:

$$P_B(s) = G_{21}(s)P_A(s) = \frac{1 + \Gamma_1(s)}{e^{\tau_1 s} + e^{-\tau_1 s}\Gamma_1(s)} P_A(s) \tag{6}$$

where τ_1 is the PTT for the first tube and Γ_1 is the reflection coefficient at the output of the first tube due to the discrepancy between the characteristic impedance of the first tube Z_{c1} and the load impedance Z_{L1} that is due to the input impedance of the second tube and the resistance R:

$$\Gamma_1(s) = \frac{Z_{L1}(s) - Z_{c1}}{Z_{L1}(s) + Z_{c1}} = \frac{R//Z_{i2}(s) - Z_{c1}}{R//Z_{i2}(s) + Z_{c1}} \tag{7}$$

where // denotes a parallel connection and Z_{i2} denotes the input impedance of the second tube and is given by [26]:

$$Z_{i2}(s) = Z_{c2}\frac{e^{\tau_2 s} + \Gamma_2 e^{-\tau_2 s}}{e^{\tau_2 s} - \Gamma_2 e^{-\tau_2 s}} \tag{8}$$

here Z_{c2} is the characteristic impedance of the second tube and τ_2 is the pulse transit time associated with the second tube. Γ_2 is the reflection coefficient at the interface of the second tube and the load given by:

$$\Gamma_2(s) = \frac{Z_L(s) - Z_{c2}}{Z_L(s) + Z_{c2}} = \frac{R_T}{2Z_{c2}R_T C_T s + (2Z_{c2} + R_T)} = \frac{\lambda_2}{s + \lambda_1} \tag{9}$$

where $\lambda_1 = \frac{2Z_{c2}+R_T}{2Z_{c2}R_T C_T}$ and $\lambda_2 = \frac{R_T}{2Z_{c2}R_T C_T}$. Next by combining $Z_{L1} = R//Z_{i2}$ with Equations (8) and (9) yields:

$$Z_{L1}(s) = \frac{Z_{c2}R[(s + \lambda_1)e^{\tau_2 s} + \lambda_2 e^{-\tau_2 s}]}{(Z_{c2} + R)(s + \lambda_1)e^{\tau_2 s} + \lambda_2(Z_{c2} - R)e^{-\tau_2 s}} \tag{10}$$

Imposing negligible wave reflection occurring to the outlet of first tube at high frequencies yields the following relationship between the characteristic (Z_{c1}) and load (Z_{L1}) impedances associated with the first tube:

$$Z_{c1} = \lim_{s\to\infty} Z_{L1}(s) = \frac{Z_{c2}R}{Z_{c2} + R} \tag{11}$$

Substituting (10) and (11) into (7), Γ_1 is obtained as follows:

$$\Gamma_1(s) = \frac{\lambda_2 R e^{-\tau_2 s}}{(Z_{c2} + R)(s + \lambda_1)e^{\tau_2 s} + \lambda_2 Z_{c2} e^{-\tau_2 s}} \tag{12}$$

Subsequently, substituting (12) into (6) yields the following $G_{21}(s)$:

$$G_{21}(s) = (Z_{c2} + R)\frac{(s + \lambda_1)e^{\tau_2 s} + \lambda_2 e^{-\tau_2 s}}{(Z_{c2} + R)(s + \lambda_1)e^{(\tau_1+\tau_2)s} + \lambda_2 Z_{c2} e^{(\tau_1-\tau_2)s} + \lambda_2 R e^{-(\tau_1+\tau_2)s}} \tag{13}$$

On the other hand, the relationship between P_B and the peripheral BP P_P is given by (5), with τ and Z_c replaced by τ_2 and Z_{c2}, respectively:

$$P_P(s) = G_{22}(s)P_B(s) = \frac{s + \lambda_1 + \lambda_2}{(s + \lambda_1)e^{\tau_2 s} + \lambda_2 e^{-\tau_2 s}} P_B(s) \quad (14)$$

Using (13) and (14), the relationship between P_A and P_P is given by:

$$P_P(s) = G_{21}(s)G_{22}(s)P_A(s)$$
$$= \frac{(Z_{c2} + R)(s + \lambda_1)e^{\tau_2 s} + \lambda_2 e^{-\tau_2 s}}{(Z_{c2} + R)(s + \lambda_1)e^{(\tau_1+\tau_2)s} + \lambda_2 Z_{c2} e^{(\tau_1-\tau_2)s} + \lambda_2 R e^{-(\tau_1+\tau_2)s}} \frac{s + \lambda_1 +}{(s + \lambda_1)e^{\tau_2 s} -} \quad (15)$$

In summary, the 2-TL model above is characterized by six parameters in total: PTT τ_1 and τ_2, bifurcation resistance R, characteristic impedance Z_{c2} (or $R_T = \frac{2\lambda_2}{\lambda_1 - \lambda_2} Z_{c2}$), and polynomial coefficients λ_1 and λ_2.

2.3: Blood Pressure Wave Propagation along the Tube-Load Model

All physical systems suffer from energy dissipation, also referred to as loss and the wave propagation dynamics in the human arterial system are no exception to this rule. The losses arise from head-loss associated with the friction of the motion of the fluid, the changes in arterial cross section as well as with bifurcations. In this study we have neglected losses since it has been shown that in major arterial pathways compliance is relatively high and losses are negligible, such pathways are the descending aorta (the prominent pathway from the central to the femoral line we have considered) and the subclavian (which is a prominent portion of the brachial line considered). It is noted that to account for the losses creating a difference in biases between the central and peripheral blood pressures these differences in mean were eliminated which overall does not alter the methodology since the tube load model has a gain of 1 at zero frequency.

Transmission line theory allows for wave specific phenomena such as the presence of static waves and wave amplification. Static waves are waves that are produced when the wavelength of the input signal takes on a specific fraction of the length of the tube, such fractions are ¼, ½, ¾ and 1. In these cases the overall wave that is seen as an observer is that of a static wave (the sum of the forward and backward traveling wave) with nodes and troughs. The heart beats at a frequency of 1 Hz and produces waves that propagate at speeds of between 1 and 3 meters per second. The wavelength of these waveforms when compared to the length of the tubes (anywhere between 0.8 to 1.5 meters) would indicate the highly unlikely event that static waves

would appear and would also rule out the possibility of resonance occurring which are not observed in the human cardiovascular system.

2.4: Data Collection Protocol

Following the approval from the University of Alberta Health Research Ethics Board (ID: Pro00021889) and informed consent from the patients, BP waveform data required to validate the tube-load models (i.e. invasive central aortic, radial and femoral BP) were collected from patients undergoing CABG with CPB. Our inclusion criteria were 1) written informed consent, 2) age 18 through 80 years, inclusive, and 3) scheduled for CABG with CPB, whereas our exclusion criteria were 1) scheduled for heart surgery other than CABG that can incur distortion of central aortic BP waveform (e.g. aortic valve repair etc.), 2) female of childbearing potential, 3) emergency surgery, and 4) body mass index (BMI) greater than 35. To acquire BP waveform data and assess the validity of the tube-load models in diverse physiologic conditions, the data were collected both before and after the CPB procedure. The rationale behind collecting BP data both before and after the CPB procedure was that prolonged anesthesia induces significant hemodynamic changes [37], and ventricular performance immediately after cardiac surgery may also be impaired. Consequently, we expected to secure data for validating the tube-load models in two distinct hemodynamic conditions per subject without introducing any exogenous interventions, e.g. administration of vasopressor drugs. The BP data were collected for the duration of 2 minutes, both before and after the CPB procedure [59].

Our experimental setup is visualized in Figure 2-4. Initially a catheter was inserted into the radial artery and the anesthesia was applied to the patient. Next a second catheter was inserted into the femoral artery and just before and following the CPB, a cannula was inserted into the aorta by a surgeon, and BP waveform recordings were obtained from all three cannula at a sampling rate of 1 kHz. Data from the BP transducers (TruWave PX, Edwards Life Sciences, CA, USA) were transmitted to a patient monitor in the operating room (IntelliVue MP90, Philips Healthcare, The Netherlands). BP waveform data were conveyed to data acquisition equipment (MP150, Biopac Systems Inc., CA, USA) using a custom-built interface cable and a blood pressure module (M1006B, Philips Healthcare, The Netherlands). The equipment was properly calibrated before the beginning of each surgical case to ensure that accurate BP data were collected [59].

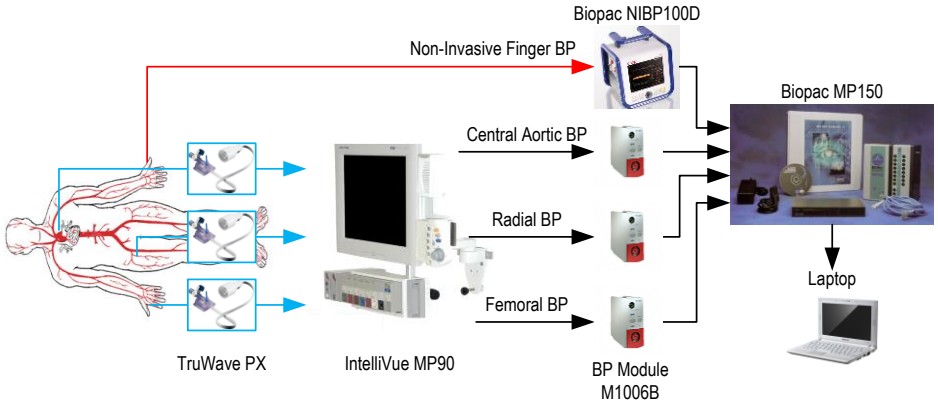

Figure 2-4 Experimental Setup - Data Collection

Hemodynamic measures of the subjects enrolled in the study are listed in Table 2-2, which indicates that the subjects were in diverse physiologic states. In particular, PTT values (which are known to largely affect the tube-load model [25, 38]) exhibited large inter-individual differences; maximum differences of 109 ms and 87 ms in the aortic-femoral PTT were observed before and after CPB, respectively. Moreover, the physiologic states of the subjects before and after CPB were greatly varied in values (see Table 2-2), though statistical significance was not established due to the small number of data. The diversity in hemodynamic conditions among different subjects made it possible to rigorously assess the validity of the tube-load models under a wide range of physiologic states. Figure 2-5 shows the radial blood pressure waveform for the first 5 subjects, the diversity in the data can clearly be seen be the dramatic differences between waveforms.

Table 2-2 Hemodynamic Measures of the Subjects used in the Validation of the Tube-Load Model

Subject ID	Pre-Cardiopulmonary Bypass					Post-Cardiopulmonary Bypass				
	HR [bpm]	MAP [mmHg]	SP [mmHg]	PP [mmHg]	PTT [ms]	HR [bpm]	MAP [mmHg]	SP [mmHg]	PP [mmHg]	PTT [ms]
1	48.0	66.6	86.2	33.6	U 118.4 L 146.8	82.2	97.4	131.8	54.1	U 77.5 L 79.3
2	68.6	69.6	92.5	38.1	U 91.4 L 102.8	80.6	60.2	79.5	32.4	U 93.9 L 127.7
3	72.0	83.5	120.9	61.4	U 87.1 L 43.4	72.0	57.1	83.8	41.1	U 97.4 L 40.5
4	78.8	68.8	85.2	29.2	U 100.5 L 82.9	85.7	72.0	95.7	37.4	U 86.7 L 71.7
5	63.4	88.3	110.5	43.3	U 65.3 L 37.4	77.1	60.2	82.5	38.2	U 71.4 L 57.1
6	56.6	98.3	141.4	69.0	U 60.3 L 48.3	85.7	77.2	100.5	36.8	U 70.4 L 64.9
7	63.4	60.9	79.6	31.8	U 86.5 L 57.1	82.3	65.2	95.2	49.0	U 76.8 L 52.7
8	54.8	56.1	80.2	41.7	U 64.6 L 75.0	58.3	50.6	80.0	48.1	U 62.9 L 65.8
Mean+/-SD	63.2+/-10.0	74.0+/-14.5	99.6+/-22.5	43.5+/-14.4	84.3+/-20.0	78.0+/-9.2	67.5+/-14.7	93.6+/-	42.1+/-7.4	79.6+/-36.7

	74.2+/-18.5	17.4	70.0+/-26.2

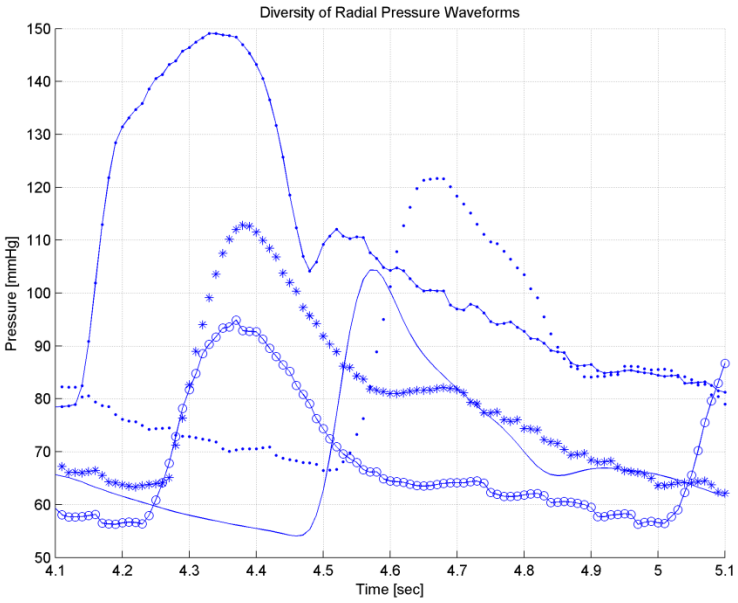

Figure 2-5 Radial Blood Pressure of First 5 Subjects

2.5: Tube-Load Model System Identification Procedure

To perform system identification, for each patient 35 second long stable central, radial and femoral blood pressures were extracted from the recordings once for pre-CPB and once for post-CPB from the original 2 minutes of data recorded and were then down-sampled to 100 Hz. Next the transfer functions were converted to their discrete-time domain equivalents, and the forward difference approximation $s \approx F_s(z-1)$ was used to estimate the continuous time models by discrete time ones. F_s denotes the sampling frequency (here 100 Hz). Using the forward difference approximation Equation (5) can be re-written as:

$$G_1(z) = \frac{z + F_s^{-1}(\eta_1 + \eta_2) - 1}{z^{n+1} + (F_s^{-1}\eta_1 - 1)z^n + F_s^{-1}\eta_2 z^{-n}} \tag{16}$$

where $n = [\tau F_s]$ is the discrete-time domain PTT and the brackets ($[.]$) denote rounding to the nearest integer digit. The estimate of the central aortic BP can be calculated from the peripheral BP using the discrete transfer function by using:

$$\hat{P}_A(k) = Z^{-1}\{G_1^{-1}(z)P_P(z)\} \tag{17}$$

Where $Z\{.\}$ is the Z-transform. The difference equation (17) can be written as:

$$\hat{P}_A(k+1) = \left[1 - \frac{(\eta_1 + \eta_2)}{F_s}\right]\hat{P}_A(k) + \psi\big(P_P(k)\big) \tag{18}$$

where $\psi(.)$ is given by:

$$\psi\big(P_P(k)\big) = P_P(k+n+1) + (F_s^{-1}\eta_1 - 1)P_P(k+n) + F_s^{-1}\eta_2 P_P(k-n) \tag{19}$$

Therefore the 1 tube load model is identified by minimizing:

$$J = \left\|P_A - \hat{P}_A\right\| = \sqrt{\sum_{k=1}^{N}\left[P_A(k) - \hat{P}_A(k)\right]^2} \tag{20}$$

Essentially the optimization problem (20) is defined as the 2-norm of the discrepancy between measured and estimated central aortic blood pressure and N is the number of data points considered. The optimization problem (20) is constrained by the fact that all physiological parameters must be bigger than or equal to zero for physiological relevance and that η_1 but be bigger than η_2, this is a trivial conclusion given the definitions of these parameters, i.e. that:

$$\eta_1 = \frac{2Z_c + R_T}{2Z_c R_T C_T} \geq \eta_2 = \frac{R_T}{2Z_c R_T C_T} \tag{21}$$

Given these constraints model identification reduces to the constrained optimization problem:

$$\Theta_1^* = \min_{\Theta_1 \in \mathrm{D}_1} J(\Theta_1) = \min_{\Theta_1 \in \mathrm{D}_1} \left\|P_A - \hat{P}_A\right\| \tag{22}$$

where $\Theta_1 = \{\tau, \eta_1, \eta_2\}$ and $\mathrm{D}_1 = \{\Theta_1 | \tau > 0, \eta_1 > \eta_2 > 0\}$.

The 2 tube load model is also identified utilizing the same procedure outlined above for the 1 tube load model, the constrained optimization is defined as:

$$\Theta_2^* = \min_{\Theta_2 \in \mathrm{D}_2} J(\Theta_2) = \min_{\Theta_2 \in \mathrm{D}_2} \left\|P_A - \hat{P}_A\right\| \tag{23}$$

where $\Theta_2 = \{\tau_1, \tau_2, \lambda_1, \lambda_2, \mathrm{R}, \mathrm{R_T}\}$ and $\mathrm{D}_2 = \{\Theta_2 | \tau_1 > 0, \tau_2 > 0, \lambda_1 > \lambda_2 > 0, \mathrm{R} > 0, \mathrm{R_T} > 0\}$.

2.6: Tube-Load Model Validity in Humans

The validity of 1 tube-load and 2 tube-load models were assessed in terms of the accuracy in the estimated central aortic BP waveforms and the fidelity of the frequency responses.

For each subject both before and after the CPB, the validity of tube-load models for central aortic-radial and central aortic-femoral arterial paths were evaluated as follows. For each arterial path, the optimal estimated central aortic BP was obtained by applying peripheral (i.e. radial or femoral) BP waveform to 1 tube-load and 2 tube-load models of the corresponding arterial path identified from (21) and (22), respectively. The accuracy of estimated central aortic BP was quantified in terms of the root-mean-squared error (RMSE), the coefficient of determination (r2 value) and the limits of agreement (via the Bland-Altman statistics) between measured versus estimated central aortic BP waveforms, systolic and pulse pressure errors, and the errors associated with measured versus identified PTT values.

In addition to central aortic BP, the frequency responses estimated by the 1 tube-load and 2 tube-load models were compared with the actual, underlying frequency responses as follows. For both 1 tube-load and 2 tube-load models, the optimal estimated frequency responses were calculated by substituting $s = j\omega$ to (5) and (15) with optimal model parameters identified from (21) and (22), respectively:

$$\begin{aligned} G_1(j\omega) &= G_1(s)|_{s=j\omega} \\ G_2(j\omega) &= G_2(s)|_{s=j\omega} = G_{21}(j\omega)G_{22}(j\omega) \end{aligned} \tag{24}$$

where $G_2(s) = G_{21}(s)G_{22}(s)$. On the other hand, the actual frequency responses were obtained as ETFE, by applying the measured central aortic and peripheral BP data to the "TFE" routine in MATLAB Signal Processing Toolbox.

The effectiveness of the 1 tube-load and 2 tube-load models were compared in terms of the metrics evaluated for the central aortic BP. The difference was regarded as statistically significant if the p value calculated by the Student's t-test was evaluated less than 0.05.

The identified model parameters associated with 1 tube-load and 2 tube-load models are summarized in Table 2-3 for both aortic-to-radial and aortic-to-femoral arterial paths, and the corresponding box plots are shown in Figure 2-6. Overall, the identified model parameters exhibited a large degree of inter-individual variability, as expected from the diversity in hemodynamic conditions observed in the data (see Table 2-2).

Table 2-3 Identified Model Parameters for the 1 Tube-Load and 2 Tube-Load Models
(a) 1-TL model (mean+/-SD)

Parameter	τ [ms]		η_1		η_2	
	Upper-Limb	Lower-Limb	Upper-Limb	Lower-Limb	Upper-Limb	Lower-Limb
Mean+/-SD	86.9±17.8	64.4±18.6	94.6±34.3	82.5±37.1	16.6±19.1	40.6±24.7

Min/Max	50/120	50/110	24.0/156.3	10.8/134.6	0.01/56.8	3.3/83.0

(b) 2-TL model (mean+/-SD)

Parameter	τ_1 [ms]		λ_1		R	
	Upper-Limb	Lower-Limb	Upper-Limb	Lower-Limb	Upper-Limb	Lower-Limb
Mean+/-SD	41.9±24.6	53.1±27.3	15.4±10.5	48.6±32.4	2.1±3.9	1.2±2.4
Min/Max	10/80	0/110	1.8/30.6	5.7/97.7	0.01/14.0	0.01/9.6
Parameter	τ_2 [ms]		λ_2		R_T	
	Upper-Limb	Lower-Limb	Upper-Limb	Lower-Limb	Upper-Limb ($\times 10^4$)	Lower-Limb
Mean+/-SD	40.6±23.2	23.8±9.6	11.5±8.6	45.4±31.3	10.7±19.9	178.5±429.9
Min/Max	10/80	10/40	1.76/29.9	3.9/95.8	5.32×10^{-4}/58.3	5.6/1771.9

Both 1 tube-load and 2 tube-load models resulted in high-fidelity representations of central aortic-peripheral arterial BP relationships. First of all, the estimated central aortic BP waveforms, both before and after CPB, were very close in morphology to their true counterparts (see Figure 2-7); on average, RMSE between true versus estimated BP waveforms were only 4.81% and 3.70% of the underlying MAP for 1 tube-load and 2 tube-load models, respectively, and the r2 values between them were also very high (see Table 2-4 and Figure 2-8). The Bland-Altman analysis indicated that the models boast negligible bias and tight limits of agreement (see Table 2-4 and Figure 2-8). In addition, PTT values identified for both 1 tube-load (τ) and 2 tube-load ($\tau_1 + \tau_2$) models were highly consistent with those measured in terms of diastolic foot-to-foot time interval [39] (see Table 2-4 and Figure 2-9). Noting that the accuracy of PTT has predominant impact on the fidelity of tube-load models [25, 39], small PTT errors as listed in Table III suggest that both 1 tube-load and 2 tube-load models were properly identified for all subjects enrolled in this study. Indeed, a representative true versus model-derived frequency responses shown in Figure 2-7 suggest that the identified tube-load models can reproduce the underlying frequency response with satisfactory accuracy, especially the location and amplitude of the first peak response that is critical for reliability of tube-load models [25]. It is noted that the frequency content of the signals produced by the heart are limited to the first 3-4 harmonics and beyond these frequencies there is essentially little to no information which is also seen in Figure 2-7 where there is a sharp reduction in the magnitude plots at frequencies above 4 Hz (the heart rate of this subject is approximately 1 Hz). In essence, the results obtained in this study strongly support the validity of 1 tube-load and 2 tube-load models in humans.

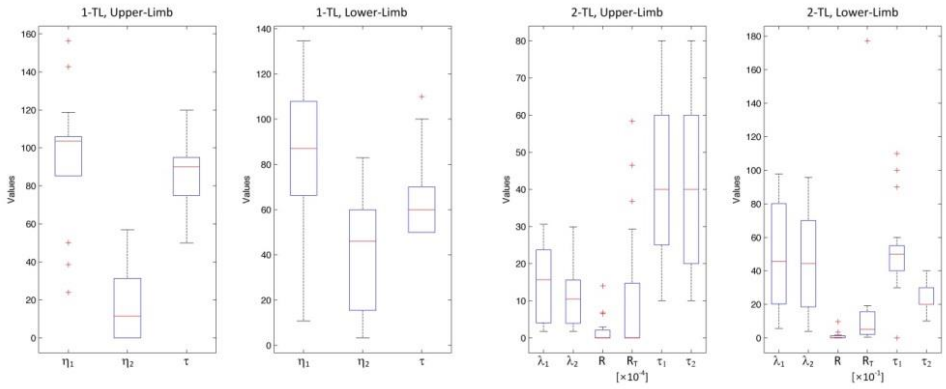

Figure 2-6 Box plot of tube-load model parameters

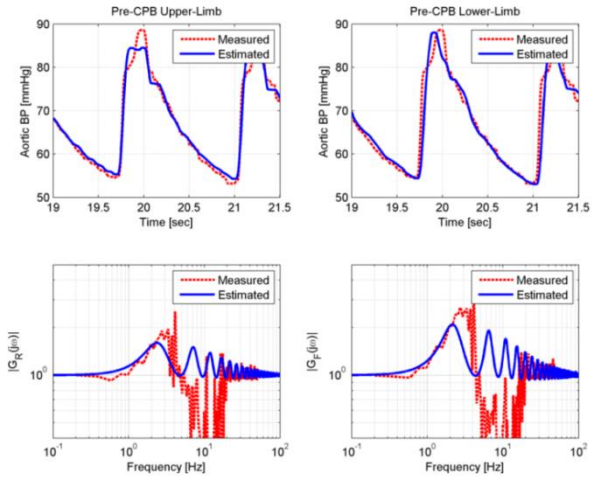

(a) 1-TL model.

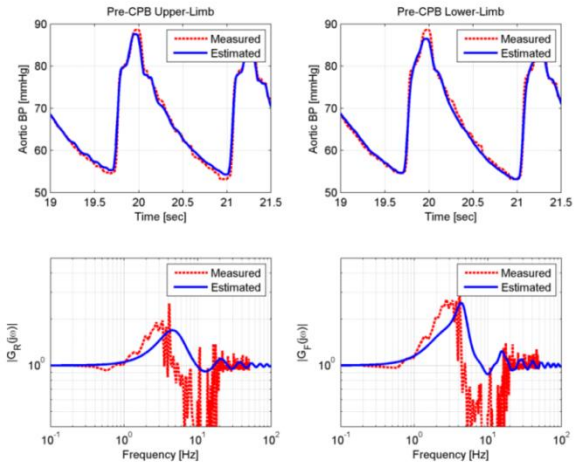

(b) 2-TL model.

Figure 2-7 Measured versus estimated central aortic BP waveforms and upper-/lower-limb frequency responses

Table 2-4 compares the metrics pertaining to central aortic BP between 1 tube-load and 2 tube-load models. First, 2 tube-load model outperformed its 1 tube-load counterpart with statistical significance ($p < 0.05$) in reproducing high-fidelity central aortic BP waveform, in that 2 tube-load model was superior to 1 tube-load model in terms of all the metrics indicative of morphological accuracy of the BP waveform including RMSE, r2 value and limits of agreement between measured versus estimated central aortic BP waveforms. In particular, RMSE was consistently smaller for 2 tube-load model than 1 tube-load model, which was expected from the fact that 1 tube-load model is a special case of 2 tube-load model. In fact, it is obvious from Figure 2-3 that 2 tube-load model reduces to 1 tube-load model by removing a tube segment (either tube #1 or tube #2) and setting $R = \infty$. Indeed, it can be easily verified that 2 tube-load model (15) reduces to 1-TL model (5) by setting $\tau_1 = 0$ and $R = \infty$, or by setting $\tau_2 = 0$ and $R = \infty$. Since the cost function associated with the model identification (21) and (22) is to minimize the RMSE discrepancy between measured versus estimated central aortic BP waveforms, 2 tube-load model (which is equipped with more tunable model parameters than its 1 tube-load counterpart) is expected to yield smaller RMSE than 1 tube-load model. Despite statistical difference, however, the amount of improvement achieved by 2 tube-load model over 1 tube-load model does not appear to be large enough to make 2 tube-load model more preferable to 1 tube-load in terms of model's practical utility (e.g. r2 value difference was only 4% on average). On the other hand, metrics related to distinct features in the BP waveform (i.e. SP, PP and PTT) were essentially comparable and were not statistically different. Note that 1 tube-load model appears to be better than 2 tube-load model in terms of PP and PTT errors (bias of the errors was smaller for 1 tube-load model; see Table 2-4), but the amount of difference was negligible when compared with the underlying values (see Table 2-2).

Table 2-4 Performance Metrics Pertaining to the 1 Tube-Load and 2 Tube-Load Models

	RMSE [mmHg]	SP Error [mmHg]	PP Error [mmHg]	PTT Error [ms]	r^2	LoA
1-TL	3.24±1.2	−1.07 ±5.17	0.19±6.85	-0.16±16.4	0.9251±0.0762	0.04±7.09
2-TL	2.52±0.9	−0.38 ±4.27	0.97±5.43	-2.66±15.0	0.9602±0.0281	0.03±5.30
p-Value	<0.05	0.24	0.22	0.32	<0.05	<0.05

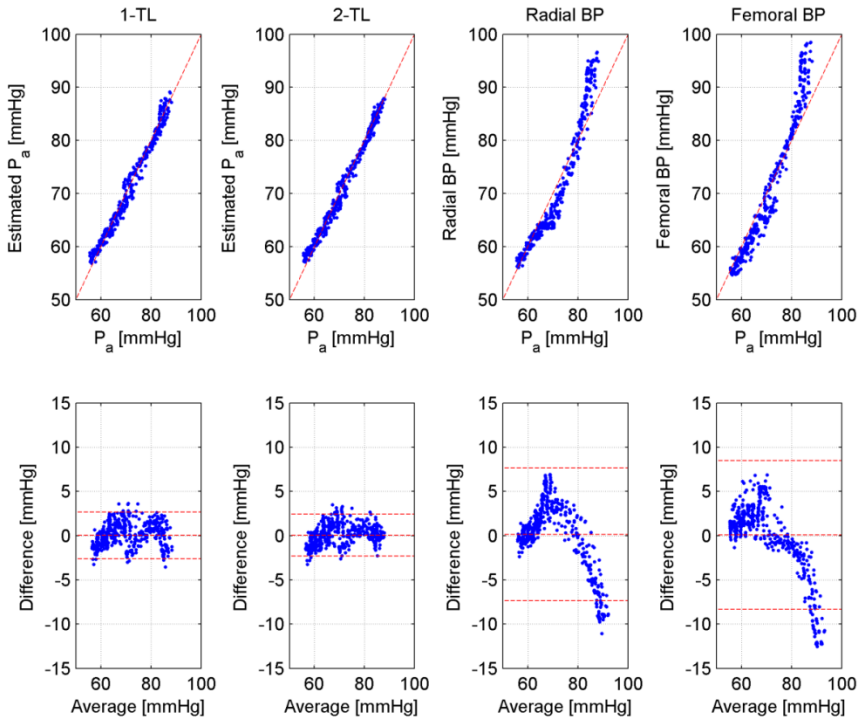

Figure 2-8 Correlation and limits of agreement between measured versus estimated central aortic BP waveforms

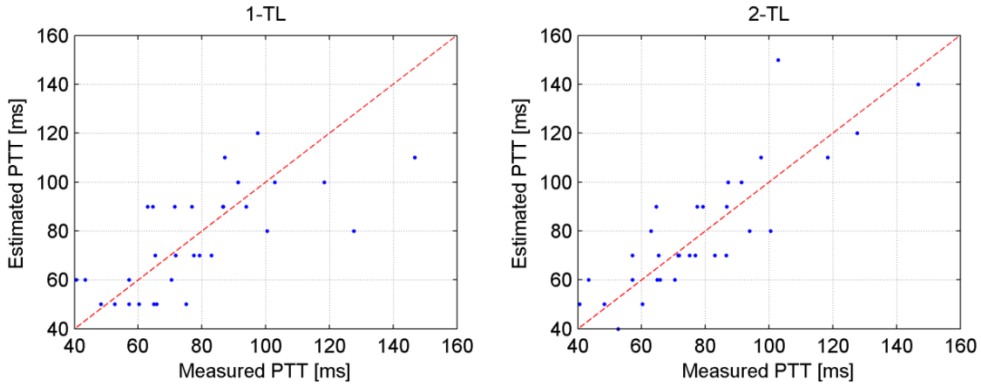

Figure 2-9 Correlation between measured versus estimated PTT values

Regardless of superior efficacy of the 2 tube-load model to reproducing the central aortic-peripheral BP relationships in comparison with 1 tube-load model, 1 tube-load model can still be regarded as a viable model based on the following observations. First, the improvement achieved by 2 tube-load model over 1 tube-load model was modest but not large (see Table 2-4). Second, 2 tube-load model sometimes tended to reduce to 1 tube-load model (in that the values of τ_1 or τ_2 assumed the lower bound

of 0 ms and R assumed very large value as indicated by the minimum values of τ_1 and τ_2 as well as the maximum value of R in Table 2-3), although the conditions on the data under which this tendency occurred (i.e. 1 tube-load model rather than 2 tube-load model sufficed to reproduce central aortic-peripheral BP relationships in the data) is still an open question. Third, the values of PTT obtained for 2 tube-load model were not always physically meaningful. In fact, PTT values for 2 tube-load model were expected to satisfy $\tau_1 > \tau_2$ since the first segment in 2 tube-load model is intended to represent the major compliant arteries (i.e. brachial and descending aortic/abdominal) in which PWV is relatively slow, considering that R is intended to represent losses due to brachial-radial and abdominal-femoral bifurcation and splanchnic organs. However, this was not always the case and often 2 tube-load models with $\tau_1 < \tau_2$ were obtained. In essence, the 2 tube-load model was superior to 1 tube-load model in fidelity, but care needs to be taken when interpreting its physiological implications.

2.7: Limitations

In terms of practical limitations, the tube-load model outlined and verified in this chapter requires blood pressure measurements recorded at two diametrically opposed limbs and these measurements need to be done invasively, which comes at a cost and risk to the patient and is difficult to perform. In the later chapters steps will be taken to develop a methodology that allows for the noninvasive measurement of peripheral blood pressures.

In regards to the quality of the data itself it is noted that the frequency content of the signal is limited to the heart rate and the first 3 to 4 harmonics of the heart rate (over 90% of the signal energy). This leaves very little to no frequency content outside of these peaks and particularly at higher frequencies but as can be seen from the results the tube-load model has been successful in in characterizing the central to peripheral blood pressures accurately and reliably, indicating a good fit of the parameters. The inherent nature of the physiological system producing and propagating the blood pressure waveforms is such that the signal is not frequency rich but should a richer signal be utilized in fitting the model it is anticipated that better parameter estimates can be achieved.

2.8: Summary

In this chapter we proposed and validated two distinct tube-load models to describe the relationship between central aortic and peripheral BP waveforms in humans. The experimental results shown indicate that both models could fit the central aortic-radial and central aortic-femoral BP waveform pairs effectively, although the 2 tube-load model was consistently superior to the 1 tube-load model with statistical significance

as far as the accuracy was concerned. Specifically, the models could estimate PTT accurately, and the model-derived frequency response was also close to the empirical transfer function estimate (ETFE) obtained directly from the central aortic and peripheral BP waveform data. We conclude that the tube-load models considered are valid representations to reproduce central aortic-radial/femoral BP waveform relationships in humans. Future work will include development and in-human validation of novel hemodynamic monitoring methods based on the tube-load models.

Chapter 3 - Validation of the Individualized Transfer Function Methodology (ITF) in Humans

3.1: Introduction to ITF and its application to Cardiovascular Health Monitoring

Substantial research effort has been put into developing methods of cardiovascular health monitoring techniques that utilize the central aortic blood pressure (CABP) due to its greater physiological and clinical relevance when compared to peripheral BP. Systolic blood pressure (SBP) and pulse pressure (PP) that are measured at the central aorta are an accurate reflection of cardiac afterload and myocardial perfusion. Also to note is that blood pressure (BP) applied to the central (compliant) arteries, as opposed to the peripheral arteries, is a major determinant of the degenerative changes that occur in hypertension and aging [23]. It has been shown that CABP, and not peripheral BP, is an independent predictor of mortality and/or cardiovascular events in geriatric patients [11], end-stage renal disease patients [10] and coronary artery disease patients [12]. Further CABP has been shown to have a stronger correlation to age [40] and better establish the seriousness of coronary artery disease [41] when compared to peripheral BP. Despite the usefulness of CABP, in practice it is difficult to measure and often involves expensive and invasive measurements that induce significant discomfort to the patient. In contrast peripheral BP can be measured both easily and safely and so has become routinely measured in practice.

Many studies have attempted to relate peripheral arterial BP (ABP) measured at distal extremities to CABP. The most well-known approach is the Generalized Transfer function whose accuracy and effectiveness has not been fully accepted [34]. Several novel approaches have recently been proposed for subject-specific estimation of CABP [25]and [42], specifically Hahn et al. [25] showed that CABP can be estimated via a cardiovascular system model derived by applying system identification to two diametrically opposed circulatory measurements (e.g. radial and femoral BPs). This individualized transfer function (ITF) approach has been validated on animal subjects to be able to estimate CABP and aortic-to-peripheral pulse transit time (PTT: equivalent to arterial distance divided by pulse wave velocity) [25].

The objective of this chapter is to demonstrate the in-human validity of the ITF approach. In order to achieve this end experimentally collected data from patients undergoing cardio-pulmonary bypass is utilized to establish the validity of ITF by showing that (i) the approach can reliably derive the cardiovascular model and (ii) it can accurately and robustly estimate the CABP. To the best of our knowledge this is the first study to experimentally evaluate the efficacy of the subject-specific

estimation of CABP method in humans. In section 2 the tube-load model of the human cardiovascular tree will be introduced and described mathematically using the framework introduced in chapter 2, next in section 3 estimation of CABP via system identification is broken down and in sections 4 and 5 results are presented and discussed

3.2: Tube-Load Model of the Cardiovascular System

The ITF methodology is based on the idea that the cardiovascular (CV) system can be modeled using two tube-load models to represent the wave propagation pathways. In this model the arterial tree is approximated by the upper and lower body tube segments. Figure 3-1 illustrates the asymmetric two tube-load model of the cardiovascular system utilized in this thesis.

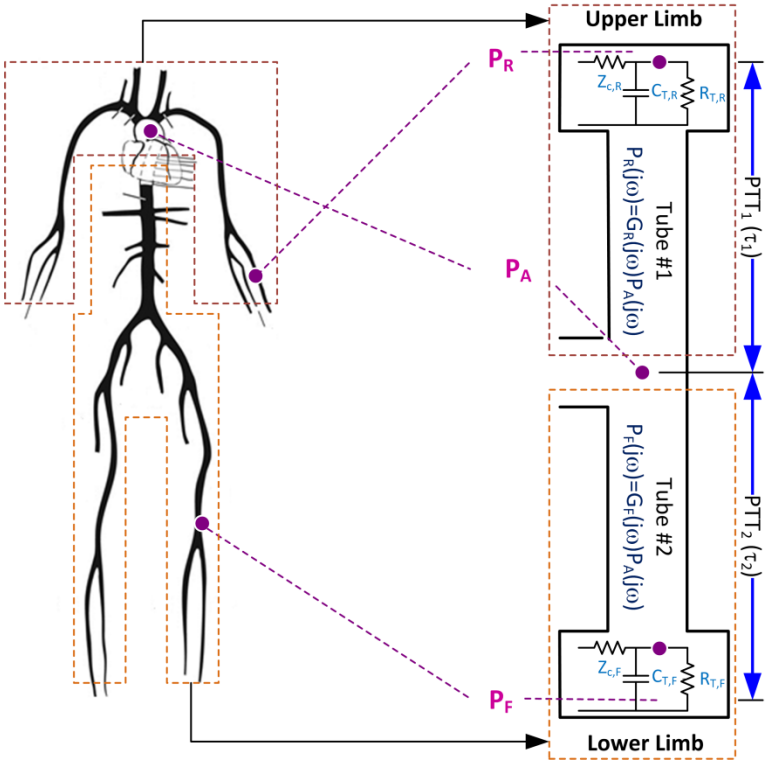

Figure 3-1 Asymmetric two tube-load model of the cardiovascular system

The tube-load models utilized in this study are assumed to be lossless and each tube has a characteristic impedance denoted by Z_c and PTT denoted by τ. Each tube is also terminated in a Windkessel load that is made up of the lumped compliance in the distal arteries (C_T), peripheral resistance exerted by the arterioles (R_T) and characteristic impedance (Z_c) to reproduce zero wave reflection at infinite frequency [29]. The mathematical model relating CABP to peripheral BP waveforms is given by:

$$P_R(s) = G_R(s)P_A(s) = \frac{s + \eta_{1R} + \eta_{2R}}{(s + \eta_{1R})e^{\tau_R s} + \eta_{2R}e^{-\tau_R s}} P_A(s)$$
$$P_F(s) = G_F(s)P_A(s) = \frac{s + \eta_{1F} + \eta_{2F}}{(s + \eta_{1F})e^{\tau_F s} + \eta_{2F}e^{-\tau_F s}} P_A(s) \quad (25)$$

where P(s) is BP, $\eta_1 = \frac{2Z_c + R_T}{2Z_c R_T C_T}$, $\eta_2 = \frac{R_T}{2Z_c R_T C_T}$, and the subscripts A, R and F are central aortic, upper-body (e.g., radial) and lower-body (e.g., femoral) locations, respectively. The model (25) is characterized by six parameters: $\Theta = \{\tau_R, \tau_F, \eta_{1R}, \eta_{2R}, \eta_{1F}, \eta_{2F}\}$.

The key reasons why two tubes have been deemed sufficient in the characterization of the human arterial tree is that:

1. System identification applied to more complicated models will involve the estimation of a larger set of parameters, which would in turn mean reduced confidence intervals of parameters (an increase in variance) and would complicate the search space unnecessarily, which would also mean that finding a minimum numerically in the search state would become increasingly difficult with the increase in level of complexity of the model.
2. In previous studies in animals it has been demonstrated that two tubes was sufficient in characterizing the subject's arterial tree dynamics and so as a preliminary step in validation of the ITF methodology the same scheme is applied to humans and if it proves ineffective then the number of tubes can be increased. In this chapter it will be shown that two tube models are sufficient for accurate and robust characterization of subject specific arterial tree models.

3.3: Estimation of CABP via System Identification

The estimation of the CABP through the ITF methodology involves a 2 step procedure: 1) identifying the cardiovascular hemodynamics which essentially boils down to the identification of the asymmetric tube-load model of the arterial tree and 2) Passing the peripheral blood pressures through the identified dynamics to estimate the CABP in a process called deconvolution. In section 3.3.1 the identification formulation, criteria for identifiability and identification procedure are outlined, next in section 3.3.2. the input deconvolution procedure and the estimation of the CABP is outlined and finally in 3.3.3 the variance analysis of the parameters is described and formulated.

3.3.1: Formulation and System Identification

The ITF methodology seeks to estimate the CABP by first identifying the arterial wave propagation pathways represented by the two tube-load models connected in parallel, next utilizing the identified dynamics and the peripheral blood pressure measurements the approach reconstructs CABP through a process called deconvolution which is essentially passing the peripheral measurements through the inverse of the identified dynamics. The key to being able to identify the arterial pathway dynamics without the original input (the CABP) is that the peripheral BPs are produced by a common source, the CABP so ITF seeks to exploit this commonality and it can be concluded that:

$$G_R^{-1}(s)P_R(s) = P_A(s) = G_F^{-1}(s)P_F(s) \tag{26}$$

Equation (26) indicates that the transfer functions characterizing the upper and lower segments of the arterial tree ($\mathrm{G_R(s)}$ and $\mathrm{G_F(s)}$ respectively) can be determined by solving the following constrained optimization problem:

$$\frac{(s+\eta_{1R})e^{\tau_R s}+\eta_{2R}e^{-\tau_R s}}{s+\eta_{1R}+\eta_{2R}}P_R(s) = \frac{(s+\eta_{1F})e^{\tau_F s}+\eta_{2F}e^{-\tau_F s}}{s+\eta_{1F}+\eta_{2F}}P_F(s) \tag{27}$$

where the expressions for the tube-load model introduced in (2) have been used to characterize the transfer functions in terms of the parameters pertaining to the tube-load models. Equation (27) can naturally be formulated into the following cost function for system identification via optimization:

$$J = \left\| \frac{(s+\eta_{1R})e^{\tau_R s}+\eta_{2R}e^{-\tau_R s}}{s+\eta_{1R}+\eta_{2R}}P_R(s) - \frac{(s+\eta_{1F})e^{\tau_F s}+\eta_{2F}e^{-\tau_F s}}{s+\eta_{1F}+\eta_{2F}}P_F(s) \right\|_2 \tag{28}$$

which can be minimized over the set of unknowns given by:

$$\Theta = \{\tau_R, \eta_{1R}, \eta_{2R}, \tau_F, \eta_{1F}, \eta_{2F}\} \tag{29}$$

which yields:

$$\Theta^* = \{\tau_R^*, \eta_{1R}^*, \eta_{2R}^*, \tau_F^*, \eta_{1F}^*, \eta_{2F}^*\} = \arg\min_{\Theta \in \mathbf{D}} J(\Theta) \tag{30}$$

where Θ^* is the optimal parallel tube-load model parameters, D is the parameter.

Three physiological constraints can be applied to the optimization problem defined in (30). These constraints can be incorporated into the system identification procedure as follows:

1. Due to the fact that the valley of the BP waveform is the most reliable and robust segment of the waveform in regards to distortions caused by wave reflection, it is assumed that the difference in PTT in the upper a lower BP

measurements is equal to the temporal difference between the two valleys of the peripheral blood pressures and can be described by the relationship:

$$\tau_d = \tau_F - \tau_R \tag{31}$$

where τ_d is the "differential" time delay.

2. Due to the physiological implications of the parameters characterizing the tube-load models, they must take on positive values and so the following constraints must hold:

$$\tau_R > 0, \eta_{1R} > 0, \eta_{2R} > 0, \tau_F > 0, \eta_{1F} > 0, \eta_{2F} > 0 \tag{32}$$

3. Careful inspection of the definitions made for η_1 and η_2 dictates that:

$$\eta_1 = \eta_2 + \frac{1}{R_T C_T} < \eta_2 + \frac{1}{Z_C C_T} = 3\eta_2 \tag{33}$$

which yields the following constraints on the relative magnitudes of η_{1R} versus η_{2R} and η_{1F} versus η_{2F}:

$$\eta_{2R} < \eta_{1R} < 3\eta_{2R},\ \eta_{2F} < \eta_{1F} < 3\eta_{2F} \tag{34}$$

In order to be able to uniquely identify the parallel tube-load models based on the constrained optimization in (28) two conditions must be satisfied:

1. It is noted that (26) can be rearranged to yield a standard input-output system identification setup as in:

$$P_R(s) = \frac{G_R(s)}{G_F(s)} P_F(s) \tag{35}$$
$$= \frac{s + \eta_{1R} + \eta_{2R}}{(s + \eta_{1R})e^{\tau_R s} + \eta_{2R}e^{-\tau_R s}} \frac{(s + \eta_{1F})e^{\tau_F s} + \eta_{2F}e^{-\tau_F s}}{s + \eta_{1F} + \eta_{2F}} P_F(s)$$

Therefore solving the optimization problem set forward in (30) yields the ratio of $G_R(s)$ to $G_F(s)$. For the parallel tube-load model to be completely characterized, pole-zero cancellation must be avoided in this ratio. This condition simply means there must be no common factors between the numerator and denominator of the transfer functions characterizing the arterial pathways, in mathematical terms:

$$s + \eta_{1R} + \eta_{2R}|_{s+\eta_{1F}+\eta_{2F}=0} \neq 0 \tag{36}$$
$$(s + \eta_{1R})e^{\tau_R s} + \eta_{2R}e^{-\tau_R s}|_{(s+\eta_{1F})e^{\tau_F s}+\eta_{2F}e^{-\tau_F s}=0} \neq 0$$

Checking the condition set forward by (36) is only possible post system identification phase but it is anticipated that this condition can readily be met in the specific case of the CV system in that the load characteristics and PTTs pertaining to the tube-loads are highly distinct since the circulations in the upper and lower body are significantly different.

2. It has been shown in [25] that to decompose the ratio of $G_R(s)$ and $G_F(s)$ into its individual constituents uniquely a sufficient condition dubbed the "blind identifiability condition" has to be satisfied. Utilizing this condition on the ratio of $G_R(s)$ and $G_F(s)$ yields the following condition applied to PTT τ_R and τ_F:

$$\tau_R F_s \geq 1, \qquad \tau_F F_s \geq 1 \tag{37}$$

where F_s is the sampling frequency. As suggested by [25], (37) can be satisfied by appropriate selection of peripheral BP measurement locations and sampling frequency and acts more as a guideline then restriction imposed on the identification procedure.

3.3.2: Input Deconvolution

In section 3.3.1 the procedure to identify the asymmetric tube-load models was outlined and criteria were set forward to ensure uniqueness and reliability of the identified transfer functions relating peripheral and central BPs. In order to reconstruct the CABP an inverse filtering approach was utilized as the deconvolution technique due to the fact that the tube-load models are minimum phase [25]. Each peripheral BP measurement is inverse filtered through its corresponding transfer function and the commonality of the CABP is exploited by noting that:

$$\hat{P}_A(s) = \sigma_1 G_R^{-1}(s) P_R(s) + \sigma_2 G_F^{-1}(s) P_F(s) \tag{38}$$

where $\hat{P}_A(s)$ is the estimated CABP, and σ_1 and σ_2 are weights satisfying $\sigma_1 + \sigma_2 = 1$.

3.3.3: Asymptotic Variance Analysis: Reliability of Tube-Load Model

In section 3.3.1 and 3.3.2 the procedure for estimating CABP from peripheral BPs utilizing the ITF approach was outlined. The accuracy and reliability of the approach can be assessed by comparing estimated and measured CABPs but it is also noted that this criteria is not the only important criteria that must be checked. Through variance analysis the reliability of the estimates of the model parameters can be assessed to give an indication of the fidelity of these estimates. Due to the fact that prior

knowledge of the true model parameters is never available calculation of exact variance is not generally possible, but expected variance can be estimated as the "asymptotic" variance using model structure and measurements [43], which converges to:

$$var(\Theta^* - \Theta_0) \cong \frac{1}{N}\lambda_N(\Theta_0)S_N(\Theta_0) \\ = \frac{1}{N}\lambda_N(\Theta_0)\left[\frac{1}{N}\sum_{n=1}^{N}\frac{d\epsilon(n,\Theta_0)}{d\Theta}\frac{d\epsilon^T(n,\Theta_0)}{d\Theta}\right]^{-1} \quad (39)$$

where Θ_0 and Θ^* are the vectors of true versus estimated model parameters, N is the length of the data used for system identification, $\lambda_N(\Theta) = \frac{1}{N}\sum_{n=1}^{N}\epsilon^2(n,\Theta)$ is the variance of the measurement error ϵ, and $S_N(\Theta)$ is the inverse of the sensitivity covariance matrix. The empirical error ϵ can be defined as follows, where Θ is the vector of tube-load model parameters:

$$\epsilon(n,\Theta) = \mathcal{L}^{-1}\{G_R^{-1}(s,\Theta)P_R(s) - G_F^{-1}(s,\Theta)P_F(s)\} \quad (40)$$

where $\mathcal{L}^{-1}$ is the inverse Laplace transform. As noted previously the variance in (40) is not computable since it is evaluated at Θ_0 (which is unknown in most real-world problems). However, the following empirical approximation using the estimate Θ^* suffices in many real-world problems:

$$var(\Theta^* - \Theta_0) \cong \frac{1}{N}\lambda_N(\Theta^*)S_N(\Theta^*) \quad (41)$$

Using the parametric asymptotic variance $\mathrm{var}(\Theta^* - \Theta_0)$ thus obtained, the variance associated with the estimation of tube-load models $G_R(s)$ and $G_F(s)$, $\mathrm{var}\left(G_i(e^{j\omega},\Theta^*) - G_i(e^{j\omega},\Theta_0)\right)$, $i = R, F$, can be obtained as follows [43]:

$$var\left(G_i(e^{j\omega},\Theta^*) - G_i(e^{j\omega},\Theta_0)\right) \\ \cong \frac{dG_i^T(e^{j\omega},\Theta^*)}{d\Theta}var(\Theta^* - \Theta_0)\frac{dG_i(e^{-j\omega},\Theta^*)}{d\Theta} \quad (42)$$

3.4: Methods

3.4.1: Experimental protocol

The experimental protocol is the same as outlined in chapter 2 but will be reiterated for the purpose of completeness. After receiving approval from the University of Alberta Health Research Ethics Board (ID Pro00021889), BP waveform data required to assess the ITF approach (invasive CABP plus radial and femoral BP) were collected simultaneously from thirteen patients undergoing cardiac surgery with cardiopulmonary bypass (CPB). Noting that prolonged anesthesia induces significant

hemodynamic changes [37], and also that ventricular performance immediately after cardiac surgery may also be impaired, data were collected both before and after CPB to assess the validity of the ITF approach under diverse physiologic conditions. The data were collected for the duration of 2 min at a sampling rate of 1 kHz. The data was then downsampled to 100 Hz to lower the computational costs of the optimization.

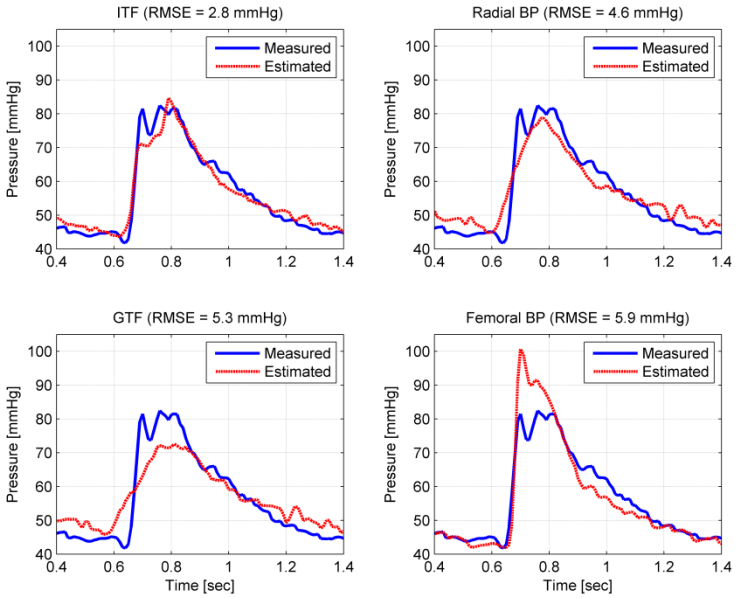

Figure 3-2 ITF approach: measured versus estimated CABP (Subject #3, post-CPB). Solid: measured CABP. Dashed: estimated CABP.

3.4.2: Validity of the ITF Approach

Data taken from the subjects was applied to the ITF approach as outlined in the previous sections and the calculated errors in relation to CABP and its estimate are summarized in Table II. This table also includes the direct peripheral BP and the GTF approach as estimates of the CABP to provide a measure of accuracy. A representative snapshot of measured versus estimated CABP is illustrated in Figure 3-2 comparing the estimations made from each approach. The ITF approach could reliably and accurately reproduce CABP and when compared to radial and femoral BP, it improved RMSE in CABP waveform by 34% and 42% ($p<0.05$), SP errors by 67% and 76% ($p<0.05$), and PP errors by 78% and 85% ($p<0.05$), respectively. Noting that radial BP is closer in morphology to the CABP, it is expected that the ITF methodology will have greater improvement over femoral BP estimates then Radial BP estimates as can be seen from the table. The ITF approach also showed benefit over the GTF approach, with 44% and 75% improvements in SP and PP errors ($p<0.05$) in addition to a moderate improvement in RMSE (11% percentagewise;

though statistically significant difference could not be established with the sample size).

In order to ensure the satisfaction of the identifiability conditions (36) and (37) were evaluated numerically using the optimal solutions found from the ITF approach, and held for all patients, both pre- and post-CPB. The asymptotic variance analysis indicated that the parallel tube-load model was determined reliably as far as CABP is concerned. It was also noted that not all the tube-load model parameters can be identified reliably. Specifically the analysis showed that η_{1R} was the most difficult to identify by the ITF approach prompted by the fact that it involves the largest asymptotic variance.

Table 3-1 Physiologic envelope of the cardiac surgery patients. PTT is shown for both central aortic-radial and central aortic-femoral paths.

Subject ID (Age/Sex)	Pre-Cardiopulmonary Bypass					Post-Cardiopulmonary Bypass				
	HR [bpm]	MAP [mmHg]	SP [mmHg]	PP [mmHg]	PTT [ms]	HR [bpm]	MAP [mmHg]	SP [mmHg]	PP [mmHg]	PTT [ms]
1 (61/M)	48.0	66.6	86.2	33.6	118.4/146.8	82.2	97.4	131.8	54.1	77.5/079.3
2 (51/M)	68.6	69.6	92.5	38.1	091.4/102.8	80.6	60.2	79.5	32.4	93.9/127.7
3 (63/M)	72.0	83.5	120.9	61.4	087.1/043.4	72.0	57.1	83.8	41.1	97.4/040.5
4 (52/F)	78.8	68.8	85.2	29.2	100.5/082.9	85.7	72.0	95.7	37.4	86.7/071.7
5 (79/F)	63.4	88.3	110.5	43.3	65.3/037.4	77.1	60.2	82.5	38.2	71.4/057.1
6 (58/F)	56.6	98.3	141.4	69.0	060.3/048.3	85.7	77.2	100.5	36.8	70.4/064.9
7 (77/M)	63.4	60.9	79.6	31.8	086.5/057.1	82.3	65.2	95.2	49.0	76.8/052.7
8 (78/M)	54.8	56.1	80.2	41.7	064.6/075.0	58.3	50.6	80.0	48.1	62.9/065.8
9 (53/M)	82.3	76.6	90.0	21.5	054.5/069.3	81.3	70.2	86.9	30.0	70.0/069.3
10 (59/M)	65.1	-*	-*	-*	-*	82.3	80.8	111.0	50.0	64.4/093.5
11 (61/M)	61.7	68.4	87.9	34.6	069.0/071.9	85.7	68.6	91.7	38.1	53.6/078.0
12 (69/M)	53.1	72.3	96.6	42.7	35.0/041.5	84.2	84.9	108.4	45.5	23.0/027.3
13 (65/M)	60.0	83.4	108.5	46.8	55.3/070.0	85.7	55.9	75.5	32.3	39.1/045.0
Mean+/-SD	63.6 ±9.9	74.4 ±11.6	98.3 ±17.9	41.1 ±12.8	74.1 ±22.1 70.5 ±29.4	80.2 ±7.4	69.3 ±12.7	94.0 ±15.2	41.0 ±7.4	68.2 ±20.0 67.1 ±24.4

Table 3-2 CABP estimation performance: ITF versus peripheral BP and GTF (mean+/-SD). LoA: limits of agreement.

			ITF	Radial BP	Femoral BP	GTF
Waveform RMSE		[mmHg]	3.7+/-1.5	5.6+/-2.2	6.3+/-2.7	3.8+/-1.9
		[%]	5.0+/-1.8	7.7+/-2.6	9.1+/-4.7	5.6+/-3.0
Systolic BP*	Bias	[mmHg]	-2.8	-8.6	11.9	3.5
	LoA	[mmHg]	-12.2/6.6	-27.6/10.4	-12.2/36.0	-8.3/15.3
Pulse BP*	Bias		-1.7	-7.7	-11.4	6.7
[mmHg]			-12.5/9.1	-30.6/15.2	-39.2/16.4	-8.6/22.0

LoA [mmHg]	

3.4.3: Reliability of Identified Tube-Load Model

In order to gauge the reliability of the identified tube-load models asymptotic variance analysis was performed on the identified tube-load model parameters and the resulting models as well as the frequency responses of the respective transfer functions, the results of which are summarized in Table 3-3. The nominal magnitude responses and corresponding confidence intervals of the upper and lower body tube-load models for subject 1 have been plotted in Figure 3-3 as an example. The estimets of the tube-load model parameters made with $N = 2000$ were found to be reliable with acceptable variance (on the average, less than 16% for η_{2R} and even smaller for the other parameters) but as noted previously η_{1R} exhibited relatively large variance. Despite this large variance in η_{1R} the overall variance in frequency response is reasonably small, indicating that the large variance associated with η_{1R} does not affect the reliability of the overall frequency response of the tube-load model to any significant extent.

Table 3-3 Reliability of parallel tube-load models as asymptotic variance (N=2000). The asymptotic variance of the tube-load model is quantified at the frequency ω_0 associated with the peak amplitude response.

(a) Tube-load model parameters (mean+/-SD)

	η_{1R}	η_{2R}	τ_R	η_{1F}	η_{2R}	τ_F
$\sqrt{var(\theta^* - \theta_0)}$	2.21+/-2.36 (202+/-235%)	0.58+/-0.97 (15.7+/-13.8%)	3×10^{-4}+/-8×10^{-5} (0.7+/-0.4%)	4.30+/-4.21 (11.3+/-16.0%)	2.71+/-2.67 (6.4+/-4.9%)	3×10^{-4}+/-8×10^{-5} (0.58+/-0.3%)

(b) Tube-load model (mean+/-SD)

	$G_R(j\omega_0)$	$G_F(j\omega_0)$
$\sqrt{var\left(G_j(z,\Theta^*) - G_j(z,\Theta_0)\right)}$	0.02+/-0.04 (1.34+/-1.18%)	0.83+/-2.46 (9.44+/-12.46%)

The relatively large uncertainty of the η_{1R} parameter can be attributed to its weak interaction on the tube-load model's time- and frequency-domain responses. The asymptotic variance analysis showed that the values of asymptotic variance of η_{1R} were proportional to the inverse of the calculated nominal value consistently. As an example, the sensitivity of the upper-body tube-load model to its parameters (Θ_R^*) for

a patient (Subject #1) is shown in Figure 3-3. In this particular patient, the value of η_{1R} was 38.4 for pre-CPB (left panel) and 0.45 for post-CPB (right panel).

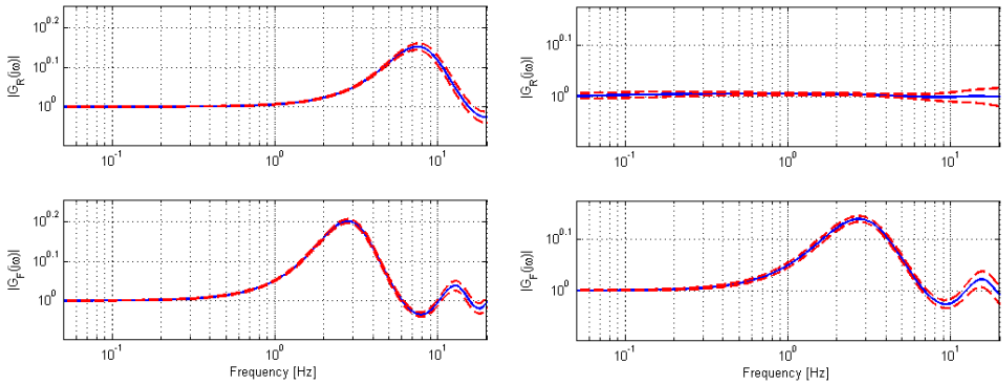

(a) Nominal amplitude frequency response (solid) and confidence interval (dashed) of parallel tube-load model. Left panel: pre-CPB. Right panel: post-CPB.

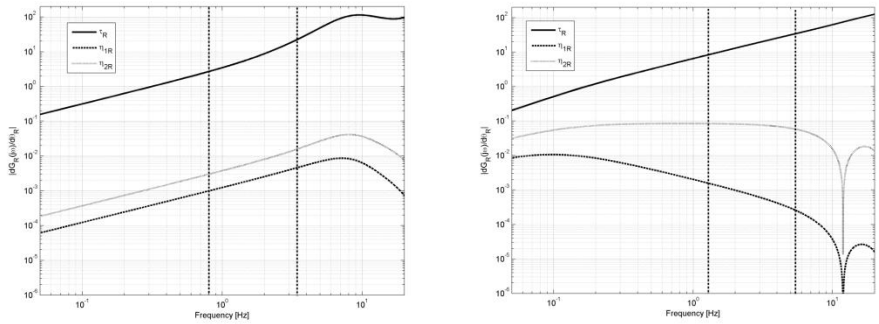

(b) Parametric sensitivity of tube-load model. Left panel: pre-CPB. Right panel: post-CPB.

Figure 3-3 ITF approach: nominal amplitude frequency response, confidence interval and parametric sensitivity of parallel tube-load model (Subject #1)

The asymptotic variance analysis yielded important observations in regards to the confidences associated with parameter identification and overall model confidence, these observations are as follows:

1. As indicated by Figure 3-3 the tube-load model frequency response is highly sensitive to the PTT which is in accordance with previous studies [44] and [45].

2. The sensitivity functions converge to zero as frequency approaches zero therefore the tube-load model loses its dependence on its parameters in the

low-frequency region. This observation is further back by (25) which indicates that tube-load model approaches a value of unity at zero frequency.

3. It is observed that the tube-load model's frequency response sensetivity to η_{2R} and η_{2F} is larger than its sensitivity to η_{1R} and η_{1F} in the mid- to high-frequency region. The sensitivity of $G_R(j\omega)$ to η_{1R} and η_{2R} are given by:

$$\frac{dG_R(j\omega)}{d\eta_{1R}} = \frac{\eta_{2R}\left(e^{-j\tau_R\omega} - e^{j\tau_R\omega}\right)}{[(j\omega+\eta_{1R})e^{j\tau_R\omega} + \eta_{2R}e^{-j\tau_R\omega}]^2}$$
$$\frac{dG_R(j\omega)}{d\eta_{2R}} = \frac{(j\omega+\eta_{1R})\left(e^{j\tau_R\omega} - e^{-j\tau_R\omega}\right)}{[(j\omega+\eta_{1R})e^{j\tau_R\omega} + \eta_{2R}e^{-j\tau_R\omega}]^2} \quad (43)$$

which demonstrates that $\left|\frac{dG_R(j\omega)}{d\eta_{2R}}\right| > \left|\frac{dG_R(j\omega)}{d\eta_{1R}}\right|$ as $\omega \to \infty$. The heart produces frequency content in the range of approximately 0.8-3.2 Hz for the left panel and 1.3-5.2 Hz in the right panel of Figure 3-3 (comprised of the principal harmonic (heart rate) and the first 3 harmonics [5]) which corresponds the mid-frequency range in which $\left|\frac{dG_R(j\omega)}{d\eta_{2R}}\right| > \left|\frac{dG_R(j\omega)}{d\eta_{1R}}\right|$ holds. Due to the range of frequency content produced by the heart it is expected that the asymptotic variances of η_{2R} and η_{2F} is smaller when compared to the asymptotic variances associated with η_{1R} and η_{1F}.

4. Inspection of the left ($\eta_{1R} = 38.4$) and the right ($\eta_{1R} = 0.45$) panels of Figure 3-3 shows that the sensitivity of the tube-load model's frequency response to η_{1R} is relatively small in the frequency envelope produced by the heart when it assumes small nominal value. Although it is expected that the asymptotic variance associated with η_{1R} will be relatively large when the nominal value is small, it was observed that for subset of data in which $\eta_{1R} > 0.5$ (which amounts to approximately 50% of the data analyzed in this study), the asymptotic variance was only 8.5% of the nominal value on the average, indicating the importance of the nominal value and significantly higher confidence levels if the condition is met that this nominal value is not extremely small.

The most important factor in estimating CABP is the overall confidence in the tube-load models which was found to be satisfactory; this can be attributed to the high reliability in the parameters excluding η_{1R} (Table 3-3 and also Figure 3-3). Given the reliability of the tube-load model, it can be argued that η_{1R} is identified with limited confidence due to its relatively negligible influence on the dynamic input-output behavior of the tube-load model (i.e., η_{1R} does not manifest itself well in the observed data).

3.5: Conclusion

In this chapter, by building on material from chapter 2, a two tube-load model of the human arterial tree was presented and described mathematically. Next the ITF approach was introduced and a thorough treatment of the identification procedure and identifiability criteria was presented. The ITF approach was implemented on data measured in-vivo from humans and the efficacy and accuracy of the estimated CABP along with confidences and variances associated with the identified parameters characterizing the arterial tree model was presented and preliminary evidence that the ITF approach may be valid for applications in humans was presented. This chapter demonstrated that the ITF methodology can accurately and reliably estimate the CABP and is indeed subject specific and does not need any a priori information in regards to the patient to achieve the CABP estimates.

3.6: Limitations and Future Work

In this study it was demonstrated that the ITF approach is capable of reproducing the CABP accurately, reliably and subject specifically. Future efforts that can be conceived to improve the ITF approach are as follows:

1. This chapter and previous study [25] highlighted that the success of the ITF approach is dependent on the frequency content of the signals that it utilizes to perform system identification. It was also observed that the frequency range that the heart produces contains a limited amount of frequency content so it is proposed that a possible solution is to apply an actuation to the arterial tree so that combined with its inherent actuation (i.e., arterial BP) the arterial tree is subject to rich and informative excitation. Chapter 4 is dedicated to this central concept.

2. The ITF approach validated in this thesis utilized invasively measured peripheral blood pressures. The efficacy of the ITF approach utilizing non-invasive arterial waveform measurements remains to be examined. Potential measurements that can yield noninvasive peripheral BP measurements are BP cuff oscillations [47] and [48] and photoplethysmography signals [49] but it is also known that the waveforms measured by these techniques is morphologically different from the underlying arterial BP waveform due to nonlinear arterial compliance and viscoelastic tissue properties (see, e.g., [50]). One possible resolution is to incorporate the non-invasive pulse waveforms in the ITF approach by extending the asymmetric two tube-load model of the arterial tree to also incorporate mathematical models of the

viscoelastic behavior of tissue and arterial dynamics and possibly the sensor itself. With the inclusion of these dynamics the identification formulation and deconvolution procedure can further be expanded to incorporate these peripheral noninvasive measurements.

3. The application of the ITF approach in a clinical setting can be in deriving cardiovascular risk parameters such as augmentation index [15], reflection magnitude and index [51] as well as aortic dP/dt [52] which can be derived from the cardiovascular system model and CABP. The applicability of the ITF methodology in deriving these risk parameters with clinically meaningful accuracy is of significant importance and our preliminary study to this end showed promise [53]. However, intensive assessment on the clinical utility of the ITF approach is yet to be conducted.

Chapter 4 - Active Noninvasive System Identification of the Human Arterial System

4.1: Introduction to Active Noninvasive System Identification with Application to the Asymmetric Tube-Load Model

In chapter 3 the "Individualized Transfer Function" (ITF) approach was validated with experimental data in humans. ITF represents an important step in the estimation of robust and reliable as well as subject specific CABP and allows for the potential improved cardiovascular health monitoring. Despite the strengths of ITF, it has been found that the technique suffers from limited persistent excitation (PE) due to the fact that the system identification procedure being implemented in the cardiovascular system. The blood pressure waveforms produced by the heart that propagate through the arterial tree are not, in general, rich enough to sufficiently excite the CV system extensively. Hahn et al. [25] proposed a quality measure that can be used to assess the model integrity based on the input signal design in the context of SYSID theory. However, unless active external perturbation is applied to the CV system, ITF inevitably suffers from the passive SYSID outcomes in that the fidelity of the arterial tree model depends significantly on the input-output data created in the CV system (i.e. central aortic and peripheral BP waveforms created by the heart). Moreover, once non-intrusive approaches are conceived for measuring the hemodynamic waveforms, additional complexity is incurred in implementing ITF due to the dynamics associated with sensors and the mechanics of tissues that can potentially exhibit highly nonlinear behaviors. Regardless, the challenges associated with non-intrusive ITF paradigm have rarely been investigated in the existing research efforts.

In this chapter a novel active non-intrusive system identification procedure to cardiovascular health monitoring is introduced. This approach utilizes a dual blood pressure cuff setup for the purpose of a collocated actuator sensor system in which actuation of the arterial tree will simultaneously be performed with measurement of internal (produced by the heart) and external (produced by the actuation of the blood pressure cuff) BPs. In this paradigm the purpose of the actuation is to produce rich transmural blood pressures to facilitate the system identification of the arterial tree. To this end a mathematical model of the propagation of arterial and cuff induced blood pressures through the arterial tree is developed and this model was used to study the effects of cuff maneuvers on transmural pressures and also to develop a methodological framework for the reconstruction of the transmural pressure waveforms from cuff oscillation measurements. In this chapter it will be demonstrated that the cardiovascular system can be excited noninvasively by active cuff maneuvers and that the transmural arterial blood pressures can be reconstructed

accurately by judicious processing of the cuff pressure oscillations. Next it is demonstrated that using noninvasively measured arterial blood pressures the ITF methodology can successfully be implemented to produce accurate and robust estimates of the central aortic blood pressure. In the final part of this chapter a system identification mathematical framework and system identification protocol is developed to utilize rich transmural blood pressures induced by the actuation of the blood pressure cuffs to produce accurate and robust noninvasive estimates of the central aortic blood pressures. Finally it is noted that the material comprising this chapter where previously presented in [60] and [61].

4.2: Preliminaries to Active Noninvasive System Identification Approach

The cardiovascular system is actuated by laterally propagating BP waves that excite arterial vessels radially. In the absence of any extra-vascular excitation source, the arterial BP waveform is the only source of excitation for the CV system but it is know that this signal is seriously limited in frequency contents (see Figure 4-1a). Therefore, it is highly likely that arterial BP wave cannot yield rich input-output data appropriate for CV SYSID. The proposed methodology dubbed the Active Non-intrusive CV SYSID approach aims to resolve the challenge of limited frequency content by externally exciting the arterial tree to obtain rich trans-mural pressure waves that propagate through the CV system (see Figure 4-1b). The central theme is to consider that the CV system is modeled as a wave propagation system that is excited by the trans-mural pressure (the difference between intra and extra-vascular pressures) acting on the arterial tree, and given this if extra-vascular pressures is properly designed and super-imposed upon the arterial BP wave then this methodology can potentially yield persistently exciting trans-mural pressure waves that can significantly enhance the efficacy of CV SYSID by providing additional frequency content. It is noted that the CV system under external excitation can be regarded as the more general case of that of the nominal CV system under the assumption that the linear superposition principle holds and it is noted that Figure 4-1a can be obtained from Figure 4-1b simply by removing the extra-vascular excitation.

4.3: Modeling of Pressure Waveform Propagation

The pressure waveforms produced by the heart and by the blood pressure cuff propagate both through the arterial tree and through tissue and cuff material. There is a clear distinction and the dynamics of each of these propagations needs to be described accordingly.

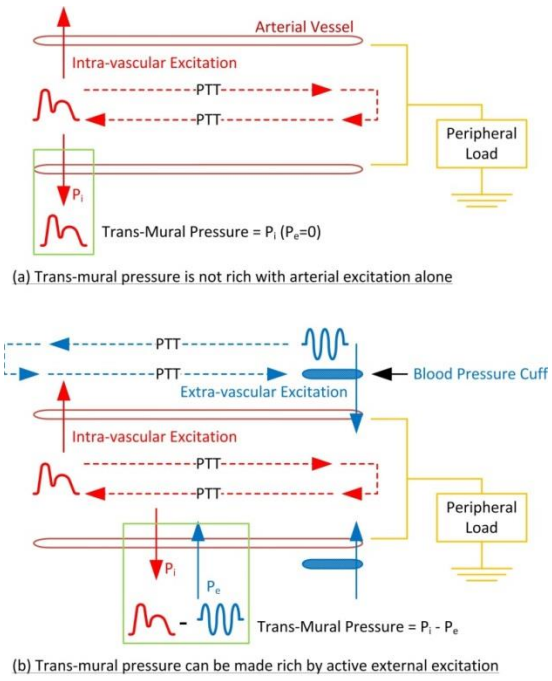

Figure 4-1 Cardiovascular SYSID Using Rich Transmural Pressure Waveforms Via Active and Noninvasive Extra-Vascular Excitation

4.3.1: Pressure wave propagation in the CV system (arterial tree):

In this preliminary feasibility study, we used the asymmetric T-tube model [29] to model the behavior of arterial tree and its wave propagation mechanics in response to the intra- and extra-vascular pressures. The upper and lower-body circulations are modeled by uniform lossless transmission lines terminated with Windkessel-type loads. In this setup the CV system is driven by 2 inputs: 1) the central aortic BP P_0 created by the heart and 2) the extra-vascular excitation pressures P_{e1} and P_{e2} acting on the upper- and lower-body locations. The arterial pathways for wave propagation are characterized by the reflection coefficients at the peripheral ends Γ_1 and Γ_2 which are defined by (8), the PTT of each tube τ_1 and τ_2 and the reflection coefficient at the proximal ends (Γ) which are assumed to be unity. This assumption is made based on the state of the aortic valve where during full closure it is hypothesized that perfect reflection occurs but this approximation may not be realistic for systole. Finally in order to calculate transmural blood pressures the extra-vascular pressures and the intra-vascular pressures at proximal and peripheral locations are subtracted at their respective locations (denoted as $P_{TM,0}$, $P_{TM,1}$ and $P_{TM,2}$ in Figure 4-2).

The trans-mural pressure at any location in the CV system is contributed by the intra-vascular (arterial) BP and the extra-vascular excitations applied at peripheral locations:

$$P_{TM,j} = P_j - P_{E,1j} - P_{E,2j} \tag{44}$$

where P_j is the intra-vascular pressure, while $P_{E,1j}$ and $P_{E,2j}$ are the extra-vascular pressures due to the excitation applied to upper- and lower-body peripheral locations, respectively. From the development in chapter 2 the relationship among P_0, P_1 and P_2 can be expressed in terms of PTT τ_j and reflection coefficient Γ_j:

$$\begin{aligned} P_1(s) &= G_1(s)P_0(s) = \frac{1+\Gamma_1(s)}{e^{\tau_1 s} + e^{-\tau_{1s}}\Gamma_1(s)} P_0(s) \\ P_2(s) &= G_2(s)P_0(s) = \frac{1+\Gamma_2(s)}{e^{\tau_2 s} + e^{-\tau_2 s}\Gamma_2(s)} P_0(s) \end{aligned} \tag{45}$$

where $G_j(s)$, $j = 1,2$ are the transfer functions dictating the propagation of pressure waves whose reflections occur at the peripheral location j. In order to develop wave propagation equations for the extra-vascular excitation P_{ej} we note that P_{ej} is essentially the forward wave component of the total extra-vascular wave that travels towards the heart, it is subsequently reflected at the heart due to the aortic valve and propagates back to the peripheral excitation location. Due to the assumption that the tubes are lossless, P_{ej} is simply delayed by PTT when it arrives at the heart ($P_{ej}e^{-\tau_j s}$) and the backward (reflected) component of the extra-vascular wave at the heart is assumed to be the same as its forward counterpart due to the assumption that wave reflection at the heart is perfect ($\Gamma P_{ej}e^{-\tau_j s} = P_{ej}e^{-\tau_j s}$). The backward extra-vascular wave thus obtained is delayed by PTT when it arrives back at the peripheral excitation location ($P_{ej}e^{-2\tau_j s}$).

Consequently, the composite extra-vascular wave at each peripheral location that is incurred by the excitation at the corresponding location can be expressed as follows:

$$\begin{aligned} P_{E,11}(s) &= P_{e1}(s)(1 + e^{-2\tau_1 s}) \\ P_{E,22}(s) &= P_{e2}(s)(1 + e^{-2\tau_2 s}) \end{aligned} \tag{46}$$

Finally, extra-vascular excitation created by an external source in one tube not only impacts the trans-mural pressure at the proximal end of the corresponding tube, but also propagates to and affects the other tube as follows. First, P_{ej} propagates to the heart location to yield forward and backward waves that are identical, i.e. $P_{ej}e^{-\tau_j s}$. Therefore, the composite extra-vascular wave at the proximal end of the tube incurred by P_{ej} is $2P_{ej}e^{-\tau_j s}$ (see Figure 4-2):

$$\begin{aligned} P_{E,10} &= 2P_{e1}(s)e^{-\tau_1 s} \\ P_{E,20} &= 2P_{e2}(s)e^{-\tau_2 s} \end{aligned} \tag{47}$$

These composite waves are then mapped to the peripheral ends of the other tubes via the transfer functions $G_1(s)$ and $G_2(s)$:

$$\begin{aligned} P_{E,12} &= G_2(s) \cdot 2P_{e1}(s)e^{-\tau_1 s} \\ P_{E,21} &= G_1(s) \cdot 2P_{e2}(s)e^{-\tau_2 s} \end{aligned} \tag{48}$$

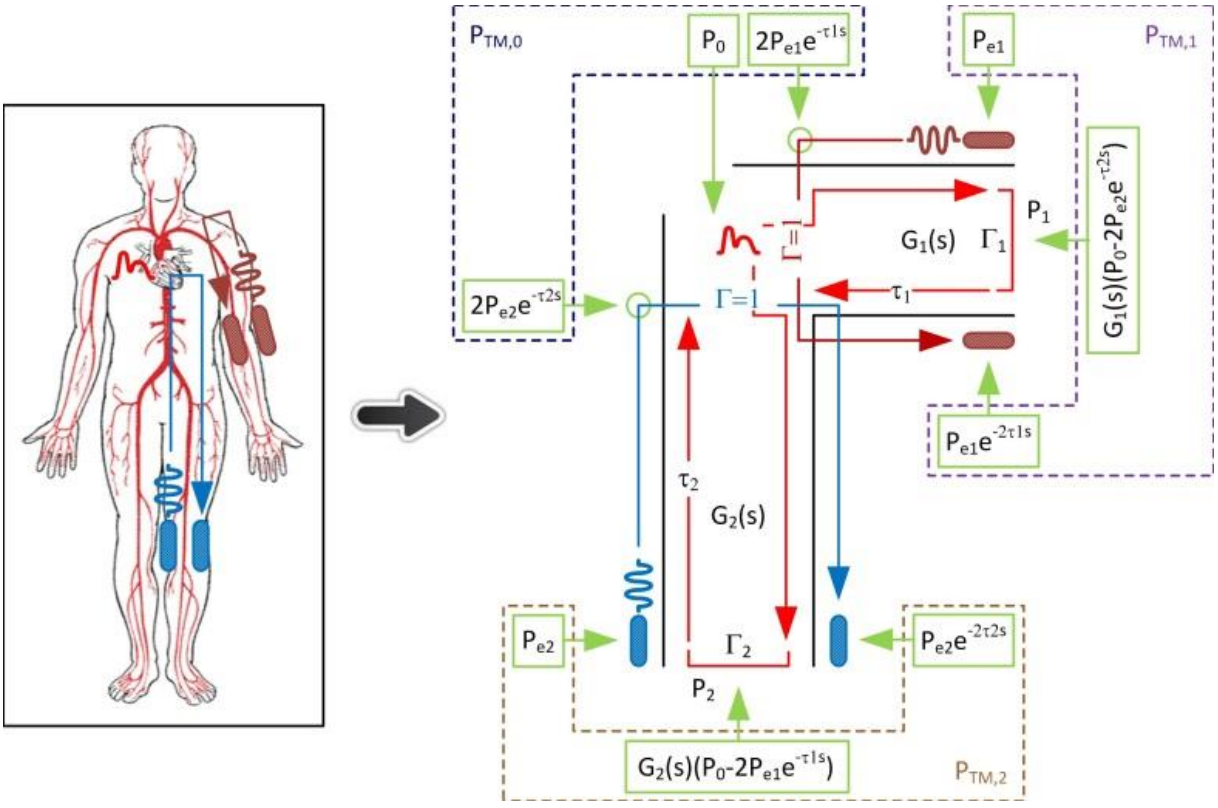

Figure 4-2 Propagation of intra- / extra-vascular BP in cv system approximated by t-tube model

The expressions for the trans-mural pressures at proximal and peripheral ends (i.e. $P_{TM,0}$, $P_{TM,1}$ and $P_{TM,2}$) can be obtained by substituting Equation (45) through Equation (48) into Equation (44):

$$\begin{aligned} P_{TM,0} &= P_0 - 2P_{e1}e^{-\tau_1 s} - 2P_{e2}e^{-\tau_2 s} \\ P_{TM,1} &= G_1(s)[P_0 - 2P_{e2}e^{-\tau_2 s}] - P_{e1}(1 + e^{-2\tau_1 s}) \\ P_{TM,2} &= G_2(s)[P_0 - 2P_{e1}e^{-\tau_1 s}] - P_{e2}(1 + e^{-2\tau_2 s}) \end{aligned} \quad (49)$$

where the Laplace variable s for all the pressure variables was omitted for the brevity of expressions. Note that all P_{ej} terms in Equation (49) are AC waveforms; P_{ej} cannot propagate otherwise.

4.3.2: Pressure wave propagation in Tissue and BP Cuff

In this study, a dual BP cuff is used as an actuator to excite CV system and as a pressure transducer to measure trans-mural pressure waveforms at the peripheral ends of upper- and lower-body circulations where extra-vascular excitations are applied. Essentially, active BP cuff maneuver propagates into the artery through the tissue in

order to yield persistently exciting trans-mural pressure wave in the arterial tree. Besides, the oscillation of the arterial BP wave at the level of arterial vessel (i.e. arterial BP waveform) is measured by the BP cuff as small-amplitude oscillations in the cuff pressure recording (see Figure 4-3).

In order to reproduce the dynamic behavior of a BP cuff as well as the propagation of pressure waves between the cuff and the artery through the tissue, a physics-based model developed by Ursino and Cristalli [55] was extended and integrated with the arterial tree model in Equation (44)- Equation (49) so as to account for the effect of extra-vascular excitation (see Figure 4-4).

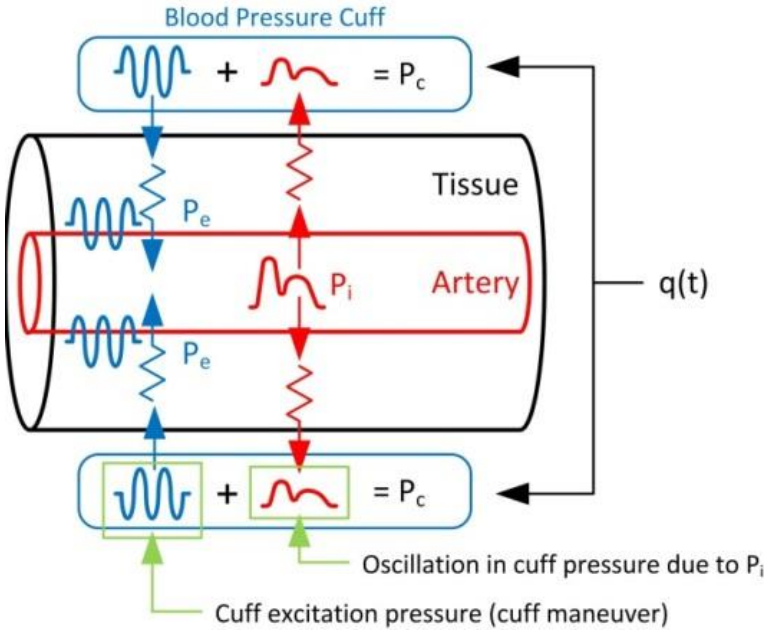

Figure 4-3 Interaction between artery, tissue and BP cuff: cuff pressure is the sum of excitation pressure of cuff and intra-vascular (arterial) pressure propagated to cuff through tissue

The cuff and tissue model for a tube j receives the equivalent intra-vascular pressure (which includes the effects of arterial BP, the extra-vascular pressure applied at the peripheral end of other tube and the extra-vascular pressure applied at the peripheral end of the tube) from the arterial tree model and the active cuff maneuver $q_j(t)$ as inputs to yield the cuff pressure P_{cj} as well as the extra-vascular pressure P_{ej} that is fed back to the arterial tree model and propagates in CV system.

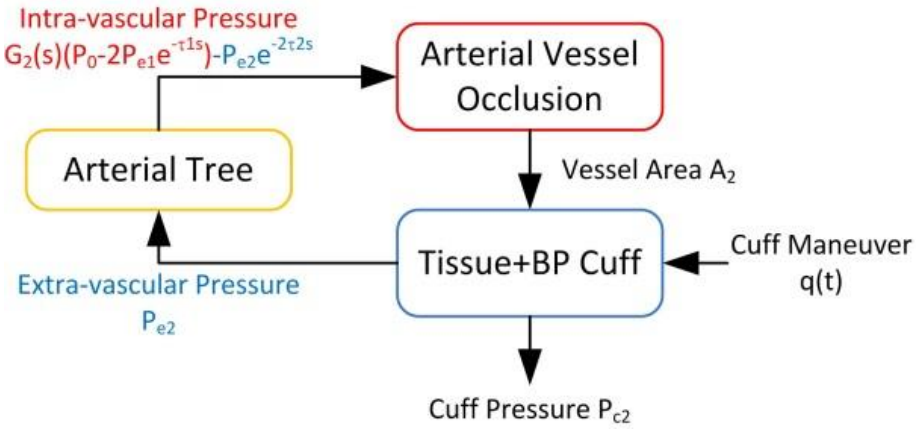

Figure 4-4 Model of integrated artery-tissue-cuff system (illustrated for lower-body circulation)

4.4: Active Noninvasive CV System Excitation

It was demonstrated in a previous study by Hahn et al. [25] that the efficacy of CV SYSID, i.e. the quality of the transfer functions $G_1(s)$ and $G_2(s)$ obtained from SYSID, depends on the input property and the underlying physiologic condition of the arterial tree. Specifically, it depends on how well the input (BP wave with its major frequency contents at heart rate) can excite the arterial tree at the frequency envelope associated with high parametric sensitivity. Generally, this frequency envelope is not known until SYSID yields $G_1(s)$ and $G_2(s)$. Regardless, it was suggested [25] that the frequency corresponding to heart rate is most often not high enough to excite the high-sensitivity frequency envelope effectively. Considering that arterial BP has a few harmonics that are significant in amplitude in addition to its fundamental heart rate frequency, the active extra-vascular excitation provided by the cuff must consist of relatively high-frequency components. Since the goal of this section is to show the preliminary proof-of-principle of the proposed approach, extra-vascular excitation in the frequency envelope of 4Hz-8Hz was considered, noting the nominal heart rate range of 60bpm-80bpm. In this frequency range, sinusoidal cuff maneuver input was applied to yield sinusoidal pressure in the cuff, which then propagates through the tissue to apply sinusoidal extra-vascular pressure on the arterial vessel (see Figure 4-3).

4.5: Noninvasive Transmural Blood Pressure Estimation

To measure trans-mural pressure, both intra-vascular and extra-vascular pressure acting upon the arterial vessel must be measured. In the context of the proposed approach, intra- and extra-vascular pressures correspond, respectively, to arterial BP and active cuff excitation pressure propagated via the tissue to the arterial vessel. First, in regards to arterial BP, it has been suggested that the arterial BP waveform

can be extracted with acceptable accuracy from the oscillations in cuff pressure under constant cuff pressure loading [56]. In this section, we propose to extract the arterial BP waveform from the measurement of cuff pressure P_{cj} $(j = 1,2)$ using a high-pass filter and calibrate the waveform thus obtained using the systolic, mean and diastolic BP measured by BP cuff. The calibration can be accomplished by the following relationship:

$$P_j(t) = \eta_2 \tilde{P}_{cj}^2(t) + \eta_1 \tilde{P}_{cj}(t) + \eta_0 \tag{50}$$

where $\tilde{P}_{cj}$ is high-frequency component in P_{cj}, i.e. P_{cj} after high-pass filtering, P_j is arterial BP waveform in tube j, and the coefficients η_i $(i = 0,1,2)$ are obtained by the relationship between $P_j(t)$ and $\tilde{P}_{cj}(t)$ at their systolic, mean and diastolic values:

$$\begin{aligned} P_{j,s} &= \eta_2 \tilde{P}_{cj,s}^2 + \eta_1 \tilde{P}_{cj,s} + \eta_0 \\ P_{j,m} &= \eta_2 \tilde{P}_{cj,m}^2 + \eta_1 \tilde{P}_{cj,m} + \eta_0 \\ P_{j,d} &= \eta_2 \tilde{P}_{cj,d}^2 + \eta_1 \tilde{P}_{cj,d} + \eta_0 \end{aligned} \tag{51}$$

where the subscripts s, m and d denote systolic, mean and diastolic, respectively.

Second, the extra-vascular pressure is created by the active cuff maneuver. Despite highly complex and nonlinear behavior of tissue and its interaction with cuff and arterial vessel, it can be proven analytically that the extra-vascular pressure is nearly identical to the pressure developed in the BP cuff via active excitation maneuver. Considering that the frequency envelope associated with the active cuff maneuver is beyond the heart rate and its non-trivial harmonics, the extra-vascular pressure can be measured with accuracy by high-pass filtering the cuff pressure recording.

Once both the intra-vascular and extra-vascular pressures are obtained as described above, the trans-mural pressures at the upper-body and lower-body cuff locations can be quantified easily by subtracting the extra-vascular from the intra-vascular pressures at the respective locations.

4.6: Excitation Measurement and Protocol Design and Results

The proposed active non-intrusive approach to CV system excitation and trans-mural pressure waveform measurement is implemented in this study with the protocol on the dual BP cuff described in detail below. To demonstrate the feasibility of the proposed approach and at the same time to keep the simplicity of presentation, active non-intrusive cuff excitation in the high-frequency regime is applied only to the lower-body circulation in this preliminary study.

1. Both upper-body and lower-body cuffs are actuated by standard maneuver (i.e. fast ramp-like increase of cuff pressure followed by slow ramp-like

decrease) so as to measure systolic, mean and diastolic BP values at the corresponding locations.

2. Both upper-body and lower-body cuffs are actuated by applying constant cuff pressures and the cuff pressures are measured. The arterial BP waveforms are extracted by high-pass filtering the cuff pressure recordings.
3. Using the systolic, mean and diastolic BP values and the corresponding levels in the arterial BP waveforms extracted from the cuff pressure recordings, unknown coefficients η_i $(i = 1,2,3)$ in Equation (50) are determined by solving Equation (51). Then the arterial BP waveforms are calibrated via Equation (50) to yield intra-vascular pressure waveforms with physically relevant scale.
4. The lower-body cuff is actuated with high-frequency sinusoidal maneuver within 4Hz-8Hz envelope, which yields active sinusoidal excitations to both upper- and lower-body arterial trees. For both upper and lower-body BP cuffs, the intra-vascular pressure waveforms are obtained by applying band-pass filtering to the cuff pressure recordings (i.e. by eliminating DC component in the low-frequency stop band and the active high-frequency excitation in the high-frequency stop band), which is subsequently calibrated using Equation (50). The extra-vascular pressure waveforms, on the other hand, are obtained by applying high-pass filtering to the cuff pressure recordings.
5. The trans-mural pressure waveforms associated with upper-body and lower-body cuff locations are obtained by subtracting extra-vascular waveforms from their respective intra-vascular counterparts.

Utilizing the 5 protocol steps outlined with the cuff maneuver sequence associated with the proposed excitation and measurement protocol is illustrated in Fig. 5 and is composed of three distinct maneuvers: standard, constant and sinusoidal maneuvers. During the standard maneuver, systolic, mean and diastolic BP of upper- and lower-body circulations are determined. During the constant maneuver, intra-vascular pressure waveforms (i.e. arterial BP waveforms) are measured and calibrated. During the sinusoidal maneuver, extra-vascular pressure acting upon the lower-body is measured, with which trans-mural pressures at both upper- and lower-body locations are obtained. To extract the arterial BP and the cuff excitation pressure waveforms from the cuff pressure recording, this study employed 9th-order Butterworth band-pass and high-pass filters with appropriate pass band and stop band frequencies.

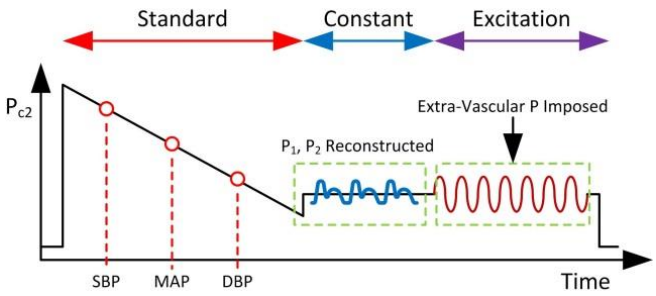

Figure 4-5 Cuff maneuver sequence for proposed excitation and measurement protocol

To establish preliminary proof-of-principle of the proposed active and non-intrusive SYSID approach, we used a synthetic arterial BP waveform (in mmHg) shown in Equation (52):

$$P_0(t) = 95 + 16\sin\left(2\pi\frac{75}{60}\,t\right) + 10\sin\left(4\pi\frac{75}{60}\,t - 1.2\right) \tag{52}$$

Figure 4-6 compares the trans-mural pressures acting upon the arterial vessels at the peripheral ends of upper- (upper panel) and lower-body (lower panel) circulations, where the right and left panels show the waveforms in the absence and presence of external excitation (4Hz sinusoidal maneuver), respectively. It is obvious that the active excitation contributes to create richer and more informative trans-mural pressure waves in the arterial tree, which have potential to enhance the quality of CV SYSID significantly.

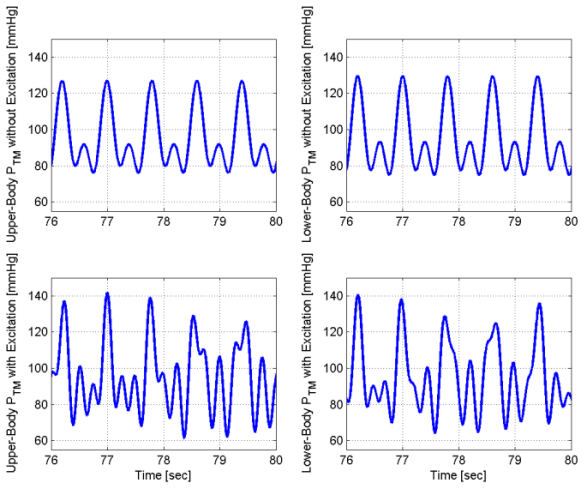

Figure 4-6 Transmural pressure waves acting on arterial vessels in the absence and presence of active extra-vascular excitation

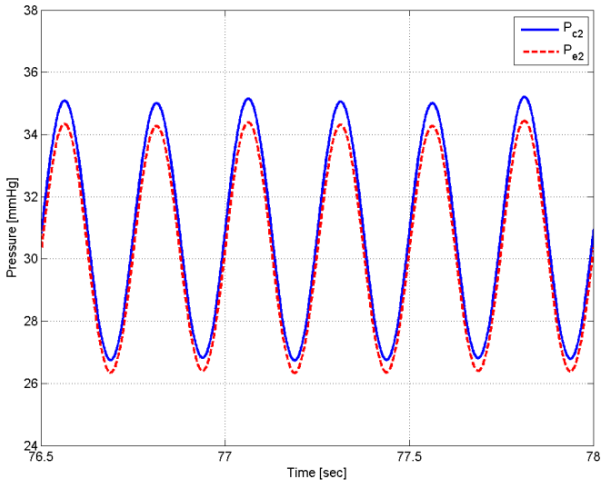

Figure 4-7 Active excitation pressure applied to BP cuff versus extra-vascular pressure acting on arterial vessel

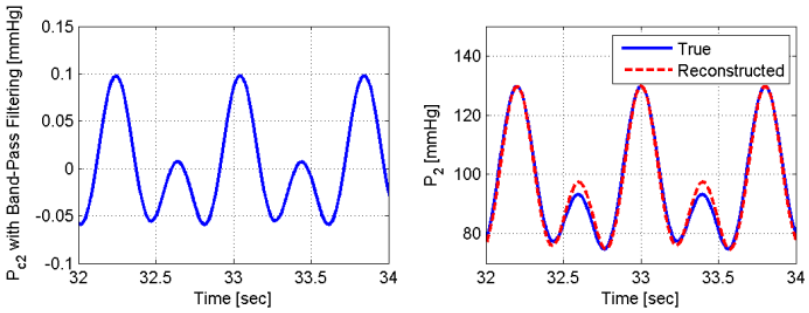

Figure 4-8 True versus reconstructed arterial BP waveforms at lower-body location

Figure 4-7 compares the extra-vascular pressure acting on the arterial vessel and the pressure incurred in the cuff by the active excitation, which demonstrates that the extra-vascular pressure acting on an arterial vessel (P_{ej}) can be measured accurately by high-pass filtering the corresponding cuff pressure (P_{cj}). In essence, there was no delay between the two waveforms. The extra-vascular pressure was different from its cuff counterpart only by a constant gain for active cuff excitation maneuvers below diastolic pressure level (resulting in positive trans-mural pressures without artery collapse). This gain was analytically evaluated to be 0.99 in this study, based on the mathematical models describing the dynamics of BP cuff, tissue and arterial vessel. Indeed, the root-mean-squared error (RMSE) between extra-vascular and cuff (after high-pass filtering was applied) pressures in Figure 4-7 was very small (0.56mmHg).

Figure 4-8 shows the arterial BP waveform extracted from the cuff pressure oscillations in the lower-body location by high-pass filtering (left panel), and the corresponding intra-vascular pressure reconstructed via the calibration in Equation (50), suggesting that intra-vascular pressure waveform can be reconstructed with

accuracy based on BP cuff. RMSE between true and measured intra-vascular pressures shown in Figure 4-8 was only 0.57 mmHg, which was only 1.82% of the underlying BP level.

Finally, Figure 4-9 shows true versus reconstructed trans-mural pressure waves at the upper-body and lower-body locations. It is important to note that, since the active non-intrusive extra-vascular excitation was applied only to the cuff in the lower-body location, the trans-mural pressures at the upper-body and lower-body locations can be expressed as follows:

$$\begin{aligned} P_{TM,1}(s) &= G_1(s)[P_0(s) - 2P_{e2}(s)e^{-\tau_2 s}] \\ P_{TM,2}(s) &= P_2(s) - P_{e2}(s)[1 + e^{-2\tau_2 s}] \end{aligned} \tag{53}$$

Consequently, lower-body trans-mural pressure waveform was obtained by subtracting extra-vascular pressure (in Figure 4-7) from intra-vascular pressure (in Figure 4-8), whereas upper-body trans-mural pressure was measured directly from its cuff pressure oscillations. For the active and non-intrusive excitation scenario shown in Figure 4-9 (4Hz sinusoidal maneuver), RMSE between the true versus reconstructed trans-mural pressure waveforms were very small; only 3.57 mmHg for upper-body and 3.76 mmHg for lower-body locations. Table 4-1 summarizes RMSE of trans-mural pressure measurement under active extra-vascular excitation of different frequencies, which clearly demonstrates the feasibility and validity of the proposed active non-intrusive approach to CV SYSID; rich and informative trans-mural pressures can be non-intrusively created and measured with fidelity.

Table 4-1 RMSE of transmural pressure under active excitations under varying frequencies

Excitation Frequency	$P_{TM,1}$ RMSE	$P_{TM,2}$ RMSE
4Hz	3.57mmHg	3.76mmHg
6Hz	3.59mmHg	4.27mmHg
8Hz	4.06mmHg	5.46mmHg

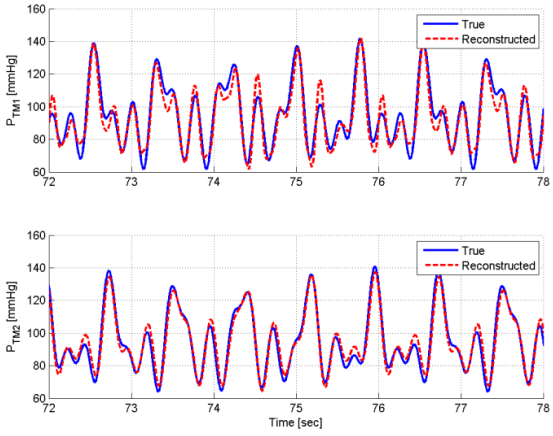

Figure 4-9 True and reconstructed trans-mural pressures acting on upper-body and lower-body arterial vessels

The most important claims from this section are that trans-mural pressure wave can be made more informative for SYSID purposes by actively exciting the extra-vascular pressure, and that it can also be measured accurately in the presence of high-frequency excitation maneuvers. Despite its initial success, this study has a few limitations.

First, the proposed approach was developed based on a simplistic approximation of arterial tree (i.e. asymmetric T-tube model extended with extra-vascular excitations). In particular, this study neglected secondary wave reflections occurring in CV system. Although it is regarded as a reasonable assumption based on a previous study on repeated wave reflections in CV system [31], the validity of wave propagation model developed in this study must be further investigated experimentally.

Second, although it is anticipated that an upper bound will exist beyond which active extra-vascular excitation is no longer effective due to the nonlinear and viscoelastic tissue dynamics, the frequency limit up to which the proposed approach is viable was not completely investigated. This study demonstrated the feasibility of the proposed active excitation idea in the 4Hz-8Hz frequency envelope (which is sufficiently high compared with nominal heart rate levels of approximately 1Hz). However, in-depth investigation on the above-mentioned concern must be clearly addressed.

Third, the excitation and measurement protocol designed in this study may further be improved. For example, the use of advanced filtering algorithms may be considered to improve the extraction of intra- and extra-vascular pressure waveforms from the cuff pressure recordings. Besides, the relationship in Equation (50) used for the calibration of intra-vascular pressure may also be improved to achieve superior intra-vascular pressure waveform measurement accuracy.

Lastly and most importantly, the effectiveness of proposed active non-intrusive extra-vascular excitation approach for CV SYSID was not completely demonstrated in the current study. It is anticipated at least intuitively that the proposed approach has potential to yield superior CV SYSID outcomes with richer and more informative input-output data pair (than mere arterial BP waveform) it can provide. The ultimate objective of this study was to establish the validity of active non-intrusive CV system excitation and trans-mural pressure measurement ideas, and as such, its efficacy in regards to CV SYSID was not the primary focus. This aspect will be intensively explored in our follow-up investigations.

4.7: Passive Noninvasive System Identification and CABP Reconstruction

It is possible to combine the dual blood pressure cuff paradigm developed in the previous section with the ITF methodology developed and validate in chapter 3 to perform noninvasive ITF, here called Passive Noninvasive ITF (PNITF). In order to demonstrate the feasibility of this approach first synthetic data was produced by using experimentally measured invasive BP signals collect based on the protocol from the previous chapters from patients undergoing cardiopulmonary bypass surgery. The peripheral blood pressures (radial and femoral) were applied to Ursino et al. [55] mathematical model of blood pressure cuff to generate synthetic cuff pressure data. The model consists of the pressure-volume relationship of the cuff bladder, the dynamics of the tissues, and the arterial vessel's hemodynamics. The cuff pressure data were then applied to the individualized transfer function algorithm to estimate central BP waveform. The protocol outlined in Section 6 to apply to the noninvasive ITF methodology as described below:

The noninvasive individualized transfer function (see Figure 4-10) measures non-invasive circulatory waveform signals and transforms them to arterial waveform signals (STEP 1), adapts its transfer function (i.e., the relationship between diametric circulatory signals) to the arterial waveform signals obtained above (STEP 2), and estimates the central BP waveform by filtering the non-invasive circulatory waveform measurements through a stable de-convolution algorithm (STEP 3). In its implementation with a dual diametric cuff system, the BP is first measured through the oscillometric procedure, and the cuffs are inflated at an appropriate sub-diastolic pressure level to measure the oscillations in the cuff pressures that correspond to the arterial pulsations. These pulsatile oscillations are then transformed to arterial BP waveforms by calibrating them to systolic, mean and diastolic BPs. Using the multiple diametric arterial BP signals thus derived, the individualized transfer function is derived by solving the following equation:

$$G_1^{-1}(s)P_1(s) = G_2^{-1}(s)P_2(s) \tag{54}$$

Where $P_i(s)$ is the ith diametric BP, and $G_i(s)$ is the transfer function relating the central BP to the ith diametric BP given by:

$$G_i(s) = \frac{s + \eta_{1i} + \eta_{2i}}{e^{\tau_i s}(s + \eta_{1i}) + e^{-\tau_i s}\eta_{2i}} \tag{55}$$

where τ_i is the pulse travel time (PTT) between central and ith diametric BP, while η_{1i} and η_{2i} are parameters related to wave reflection at the ith diametric location. Finally, the central BP waveform is estimated by processing the diametric arterial BP

waveforms by a stable de-convolution filter. In this study, a simple direct inverse filtering is used:

$$\hat{P}_0(s) = \sigma_1 G_1^{-1}(s) P_1(s) + (1 - \sigma_1) G_2^{-1}(s) P_2(s) \quad (56)$$

where $\hat{P}_0(s)$ is the estimated central BP, and $0 < \sigma_1 < 1$ is a weighting factor ($\sigma_1 = 0.5$ was used in this study). The proof-of-principle of the non-invasive individualized transfer function was established in terms of the accuracy of its estimated central BP and the reliability of the transfer function. The accuracy of the central BP was quantified in terms of the root-mean-squared error (RMSE) between true and estimated central BP waveforms, as well as the errors between true and estimated central systolic and pulse pressures. The reliability of the transfer function was quantified by the asymptotic variance of the transfer function parameters including PTT and the wave reflection coefficients.

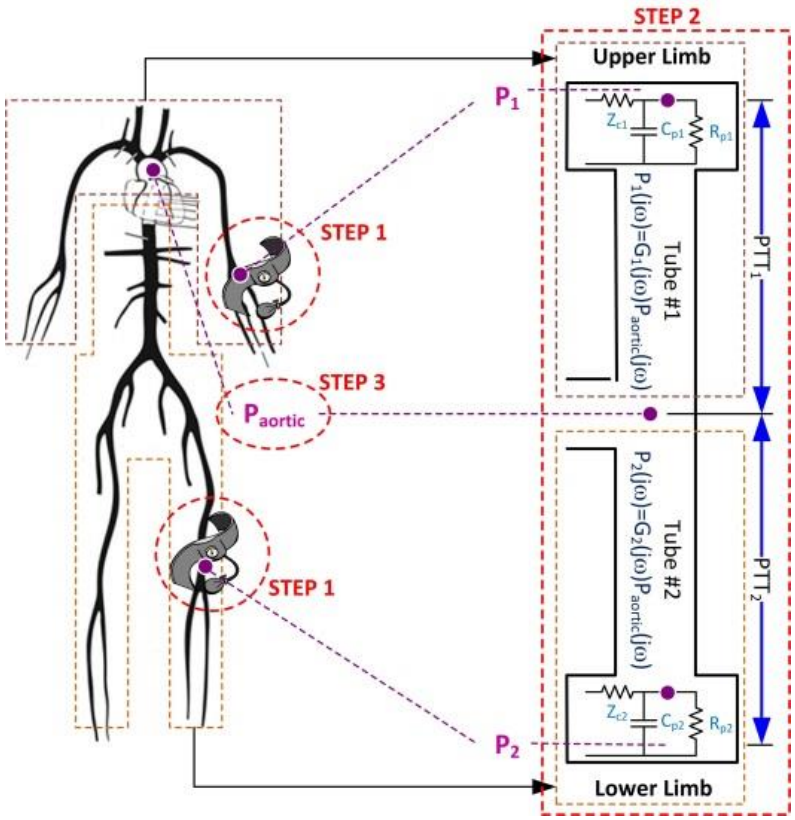

Figure 4-10 Non-invasive individualized transfer function

Figure 4-11 shows a representative example of the arterial BP waveforms derived by the non-invasive individualized transfer function. The first two plots show the diametric arterial BPs and their estimates obtained from the cuff pressure oscillations, while the third plot shows the true and estimated central BPs. The error statistics for 16 datasets, constructed from the clinical data of 8 subjects, are listed in Table 4-2. The results clearly suggest that the non-individualized transfer function can estimate

the central BP with fidelity, and it largely outperforms direct non-invasive peripheral BP in its morphologic similarity to the true central BP measurement.

Table 4-3 summarizes the asymptotic variance of PTT and the reflection coefficient parameters. Except η_{11} which suffers from relatively large uncertainty, the parameters characterizing the individualized transfer function can be regarded as reliable with tight asymptotic variance (in terms of standard deviation).

Figure 4-12 presents a representative example of the individualized transfer function's frequency response together with the amount of uncertainty involved (in terms of the confidence interval). It is noted that, despite the large variance associated with η_{11}, the frequency responses corresponding to both diametric locations exhibit small uncertainty (as suggested by their tight asymptotic variances).

Table 4-2 Accuracy of central BP estimated by the individualized transfer function. SP: systolic pressure. PP: pulse pressure

	RMSE [mmHg]	SP Error [mmHg]	PP Error [mmHg]
ITF	4.49 (6.47%)	04.06 (03.97%)	07.96 (18.12%)
P1	6.02 (8.45%)	11.84 (12.14%)	11.95 (29.23%)

In fact, the sensitivity of the individualized transfer function to η_{11} was very small, which justifies its minimal adverse impact on the fidelity of the frequency responses. Also note that non-invasively versus invasively determined transfer functions exhibit non-negligible discrepancy in their frequency responses, which appears to be mainly incurred by the limited fidelity of the arterial pulsations derived from the oscillations in the cuff pressure, which must be improved in a follow-up study.

Table 4-3 Asymptotic variance of individualized transfer function parameters: mean (SD).

τ_1 [%]	η_{11} [%]	η_{21} [%]	τ_2 [%]	η_{12} [%]	η_{22} [%]
0.94 (0.6)	67.66 (149.8)	24.19 (43.5)	0.96 (0.4)	6.97 (3.4)	3.65 (2.7)

This section demonstrated the preliminary proof-of-principle of the non-invasive individualized transfer function approach to estimating central BP waveform from non-invasive circulatory signals measured at multiple diametric locations.

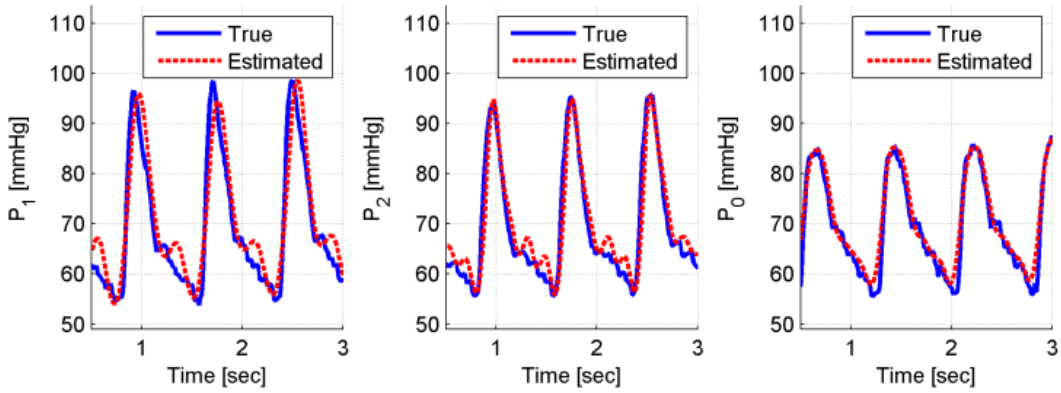

Figure 4-11 Diametric and central arterial BP waveforms derived by non-invasive individualized transfer function.

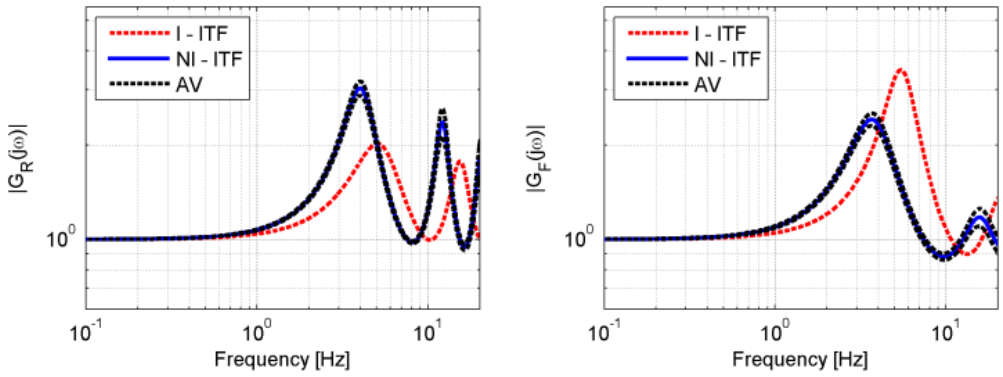

Figure 4-12 Frequency response of individualized transfer function with its confidence interval as quantified by asymptotic variance analysis.

4.8: Active Noninvasive System Identification Approach

In the ITF methodology, the dynamics of the arterial tree is identified using the arterial BP wave which excites the arterial vessels in the radial direction. The frequency contents of the arterial BP are limited to only a few harmonics of HR, and as a consequence, the arterial tree cannot be persistently excited with the arterial BP alone. Therefore, arterial BP alone cannot provide informative data to result in high-fidelity SYSID.

In the proposed active non-intrusive SYSID paradigm, the arterial tree is excited via an external actuator so that an extra-vascular pressure wave is created, which is subsequently added to the intra-vascular pressure (i.e. arterial BP) to yield a highly

informative trans-mural pressure wave. Then, the rich trans-mural pressure wave thus created is measured by the sensor collocated with the actuator. Noting that the arterial vessels are essentially excited by the trans-mural pressure wave rather than the arterial BP wave alone, extra-vascular pressures properly designed and super-imposed upon the arterial BP wave can potentially yield persistently exciting trans-mural pressure wave that significantly enhances the efficacy of cardiovascular SYSID. Note that nominal CV system not involving any extra-vascular excitation can be regarded as a special case of CV system being subject to zero extra-vascular pressure; under the assumption that the linear superposition principle holds.

The goal of the SYSID is to exploit the observations $P_{TM,1}$ and $P_{TM,2}$ (49) to identify the dynamics $G_1(s)$ and $G_2(s)$ of the CV system, and then to reconstruct the central aortic BP P_0. In this section we demonstrate that this goal can be fulfilled by exploiting the commonalty in $P_{TM,1}$ and $P_{TM,2}$: they are both affected by the central aortic BP P_0, although it is not known a priori. To exploit this commonality we conclude from (49) that:

$$P_0 = G_1^{-1}\left[P_{TM,1} + P_{e1}(1 + e^{-2\tau_1 s})\right] + 2P_{e2}e^{-\tau_2 s} \tag{57}$$

And so we can conclude that:

$$G_1^{-1}\left[P_{TM,1} + P_{e1}(1 + e^{-2\tau_1 s})\right] + 2P_{e2}e^{-\tau_2 s} = G_2^{-1}\left[P_{TM,2} + P_{e2}(1 + e^{-2\tau_2 s})\right] + 2P_{e1}e^{-\tau_1 s} \tag{58}$$

Further, to clearly illustrate the idea, we consider the scenario in which only one actuator (P_{e2}) exerts active excitation to the arterial tree (i.e., $P_{e1} = 0$). In this scenario, Equation (49) reduces to:

$$\begin{aligned} P_{TM,1} &= G_1(s)[P_0 - 2P_{e2}e^{-\tau_2 s}] \\ P_{TM,2} &= G_2(s)P_0 - P_{e2}(1 + e^{-2\tau_2 s}) \end{aligned} \tag{59}$$

both of which contains P_0. Thus, solving (59) for P_0 yields:

$$\underbrace{G_1^{-1}(s)P_{TM,1} + 2P_{e2}e^{-\tau_2 s}}_{\triangleq \psi_1(s)} = \underbrace{G_2^{-1}(s)\left\{P_{TM,2} + P_{e2}(1 + e^{-2\tau_2 s})\right\}}_{\triangleq \psi_2(s)} \tag{60}$$

In Equation (60), $G_1(s)$ and $G_2(s)$ (which are given by Equation (55)) must be determined from the observations of trans-mural pressures $P_{TM,1}$ and $P_{TM,2}$, and the active extra-vascular pressure P_{e2}. The CV dynamics $G_1(s)$ and $G_2(s)$ are characterized by PTT τ_j and the reflection coefficient Γ_j ($j = 1,2$), where Γ_j reduces to a first-order low-pass filter in case the windkessel-type load terminates the arterial conduits:

$$Z_{Lj}(s) = Z_{cj} + \frac{R_{Tj}}{R_{Tj}C_{Tj}s + 1} \rightarrow \Gamma_j(s) = \frac{\eta_{2j}}{s + \eta_{1j}} \tag{61}$$

where $Z_{Lj}(s)$ and Z_{cj} are load and characteristic impedances of the conduit, R_{Tj} and C_{Tj} are peripheral resistance and terminal compliance, all corresponding to the conduit j, and

$$\eta_{1j} = \frac{2Z_{cj} + R_{Tj}}{2Z_{cj}R_{Tj}C_{Tj}}, \qquad \eta_{2j} = \frac{R_{Tj}}{2Z_{cj}R_{Tj}C_{Tj}} \tag{62}$$

Thus, Equation (60) involves six unknowns in total to be identified:

$$\Theta = \{\Theta_1, \Theta_2\}, \qquad \Theta_1 = \{\tau_1, \eta_{11}, \eta_{21}\}, \qquad \Theta_2 = \{\tau_2, \eta_{12}, \eta_{22}\} \tag{63}$$

and the following optimization can be constituted to solve the SYSID problem in Equation (6):

$$\Theta^* = \arg\min_{\Theta \in D_\Theta} \|\psi_1(s,\Theta) - \psi_2(s,\Theta)\| \tag{64}$$

where Θ^* is the vector of optimal arterial dynamics parameters, and D_Θ is the parametric space Θ^* belongs to due to its physical implications and constraints:

$$D_\Theta = \{\Theta | \tau_j > 0, \eta_{1j} > \eta_{2j} > 0, j = 1,2\} \tag{65}$$

Indeed, PTT, η_{1j} and η_{2j} must be positive by definition. Also, $\eta_{1j} > \eta_{2j}$ is obvious from Equation (62). It is emphasized that the availability of P_{e2} is not a trivial proposition, because P_{e2} is the active excitation at the extra-vascular level but it is noted that estimation of P_{e2} has been discussed in Section 6.

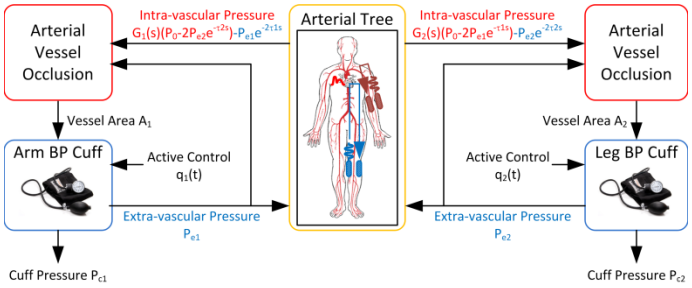

Figure 4-13 Model-based setup: integrated artery-tissue-Collocated actuator-sensor system

In this preliminary study, the feasibility of the proposed active non-intrusive CV SYSID methodology is validated in a model-based simulation experiment. The model-based setup is depicted in Figure 4-13, which consists of (i) the wave propagation in the arterial tree given by Equation (49), (ii) the change in the area of the arterial vessels due to varying trans-mural pressure and its subsequent propagation through the tissue to the skin, and (iii) the dynamics of the collocated actuator-sensor system (where a dual BP cuff is used as a prototype collocated actuator-sensor system in this preliminary study; see below for details).

In this study, a dual BP cuff is used as a prototype device for the collocated actuator-sensor system. As shown in Figure 4-13, BP cuffs are placed at the arm and leg locations to provide the excitation and observe the trans-mural pressures in these locations. The air flow $q_j(t)$ provided to the cuff controls the cuff pressure, which is subsequently propagated through the tissue to the arterial vessel and act as an active extra-vascular excitation $P_{ej}(t)$. This extra-vascular pressure propagates along the arterial tree, and is also super-imposed to the intra-vascular pressure (i.e., arterial BP) to yield the trans-mural pressure that persistently excites the arterial vessel (i.e., deforms in the radial direction) via nonlinear arterial compliance characteristic. The change in the arterial vessel area propagates through the tissue back to the cuff, which is finally observed as small-amplitude oscillations in the cuff pressure [57].

In this study, a physics-based model of the BP cuff and the dynamics of the arterial vessel loaded by the cuff developed by Ursino and Cristalli [55] was extended and integrated into the model of wave propagation in the arterial tree in Equation (49) to constitute the model-based setup to validate the proposed CV SYSID paradigm, which is capable of reproducing the dynamic behavior of the BP cuff, propagation of pressure waves between the cuff and the arterial vessel through the tissue, as well as the interaction between intra- and extra-vascular pressures. In the integrated model, the cuff maneuver is allowed to travel in the arterial tree with reflections as extra-vascular pressure, and the observed cuff pressure is allowed to accommodate the effects of the reflected extra-vascular pressures as well as the arterial BP.

For the purpose of model-based simulation experiment, the arterial BP waveforms collected from cardiac surgery patients were used. Specifically, central aortic and peripheral (radial and femoral) BP waveforms were collected from eight patients both before and after the cardio-pulmonary bypass (CPB), and were used to identify the dynamics of the arterial tree $G_1(s)$ and $G_2(s)$ corresponding to each patient. These identified dynamics were then used to simulate each patient with the corresponding peripheral BP waveform data, thereby creating the trans-mural pressures via Equation (59) (where $P_j = G_j(s)P_0, j = 1,2$ was used):

$$\begin{aligned} P_{TM,1} &= P_1 - 2G_1(s)P_{e2}e^{-\tau_2 s} \\ P_{TM,2} &= P_2 - P_{e2}(1 + e^{-2\tau_2 s}) \end{aligned} \tag{66}$$

Now the systematic procedure for the active non-intrusive CV SYSID methodology proposed in this study is summarized. The protocol required on the collocated actuator-sensor system to carry out the SYSID is depicted in Figure 4-5.

As noted previously in case of the "passive" ITF (the ITF based on the arterial BP alone), the quality of the CV SYSID heavily depends on the arterial BP (especially the HR) and the physiologic state of the arterial tree [25]. In particular, it was

observed that the arterial BP has limited capability to persistently excite the CV system, because the HR is typically lower than the frequency range in which the CV system dynamics $G_1(s)$ and $G_2(s)$ exhibit high parametric sensitivity. In this regard, the active excitation must complement the arterial BP by exciting the CV system in the relatively high frequency range to enhance the SYSID. On the other hand, the upper bound of the frequency associated with active excitation inevitably exists due to the limited bandwidth of the actuator. Noting that the arterial BP possesses up to a few significant harmonics [20], the active excitation was provided to the arterial tree in the frequency band of 20 Hz-35 Hz. In this band, the excitation maneuver was designed as the sum of ten sinusoids with random amplitudes and phase angles.

To outline the estimation of the transmural blood pressures at the peripheries we note that by definition, the trans-mural pressure is the difference between the intra-vascular and the extra-vascular pressures. In the context of the proposed SYSID methodology, the intra- and the extra-vascular pressures correspond to the arterial BP and the active excitation, respectively. Therefore, in order to derive the trans-mural pressure, both arterial BP and active excitation pressure must be determined from the available observations.

The cuff pressure P_{cj} observed by the BP cuff consists of two components: the large-amplitude oscillation corresponding to the active excitation, and the small-amplitude oscillation that represents the change in the arterial vessel area in response to the combined intra- and extra-vascular pressures acting on the arterial vessel. In case of the lower-body circulation, Equation (12b) can be decomposed into the following three components:

$$P_{TM,2} = \underbrace{P_2}_{\text{(i)}} - \underbrace{P_{e2}}_{\text{(ii)}} - \underbrace{P_{e2}e^{-2\tau_2 s}}_{\text{(iii)}} \tag{67}$$

where (ii) is the forward (i.e., traveling to the heart) component of the extra-vascular pressure created by the active excitation, whereas (iii) is its backward component traveling back to the lower-body periphery from the heart resulting from the forward component reflected at the heart. Therefore, (ii) can be inferred from the large-amplitude oscillation in P_{c2} while (i) and (iii) are included in the small-amplitude oscillation in P_{c2}. Considering that P_{e2} is nearly identical to the large-amplitude component of P_{c2} [34], and that P_{c2} is essentially known a priori through the designed active excitation maneuver, the remaining challenge in reconstructing $P_{TM,2}$ is to separate and properly calibrate (i) and (iii) from the small-amplitude component of P_{c2}.

This study proposes the following step-by-step procedure to reconstruct the trans-mural pressure $P_{TM,2}$. Firstly, the large-amplitude component of P_{c2} is extracted to

yield (ii). Secondly, the remaining small-amplitude component is band-pass filtered (with the low-frequency stop band to eliminate the DC and the high-frequency stop band to eliminate the active extra-vascular pressure) to derive the cuff pressure oscillation associated with the arterial BP, which is subsequently calibrated by (50) to yield the arterial BP (i) in the lower-body measurement site. Thirdly, the small-amplitude component is high-pass filtered to derive the cuff pressure oscillation associated with the reflected active excitation from the heart, which is scaled to have the amplitude identical to its forward counterpart (based upon the assumption that the conduit is lossless). Finally, $P_{TM,2}$ can be reconstructed by subtracting (ii) and (iii) from (i) as dictated in Equation (67).

Similarly to the lower-body case, in case of the upper-body circulation, Equation (12a) can be decomposed into two components:

$$P_{TM,1} = \underbrace{P_1}_{\text{(i)}} - \underbrace{2G_1(s)P_{e2}e^{-\tau_2 s}}_{\text{(ii)}} \tag{68}$$

where (ii) is the extra-vascular pressure, or the active excitation applied to the lower-body that has propagated to the upper-body circulation. Noting that there is no direct active excitation at the upper-body BP cuff, both (i) and (ii) in Equation (68) are included in the small-amplitude component of P_{c1}. Therefore, the trans-mural pressure $P_{TM,1}$ can be reconstructed using the following procedure. Firstly, the small-amplitude component is band-pass filtered (with the low-frequency stop band to eliminate the DC and the high-frequency stop band to eliminate the active extra-vascular pressure) to derive the cuff pressure oscillation related to the arterial BP, which is subsequently calibrated by (50) to result in the arterial BP (i) in the upper-body measurement site. Secondly, the small-amplitude component is high-pass filtered to derive the cuff pressure oscillation related to the propagated active excitation from the lower-body through the heart, which is scaled to have the amplitude identical to P_{c2} (based upon the assumption that the conduit is lossless). Finally, $P_{TM,1}$ can be reconstructed by subtracting (ii) from (i) as shown in Equation (68).

In implementing the above procedures for reconstructing the trans-mural pressures, nonlinearity associated with the BP cuff imposes a subtle challenge as to how to choose the pass band of the band-pass filter for deriving the arterial BP. Indeed, undesired harmonics are introduced to the frequency spectrum of the small-amplitude component of the cuff pressures P_{c1} and P_{c2} through the nonlinearity inherent in the BP cuff. It then distorts the frequency spectrum responsible for the arterial BP, making it difficult to discern the frequency contents associated with the arterial BP from those artifacts that are incurred by the BP cuff. In this study, two alternative approaches are proposed to resolve this challenge: (i) to retain a pre-specified number

of harmonic components in the cuff pressure oscillation, or (ii) to select the upper bound of the pass band of the band pass filter (used to extract the arterial BP) as the frequency at which the signal energy becomes a pre-specified fraction of the signal's total energy, and the harmonics below the selected bound are used to reconstruct the arterial BP, whereas those beyond it are regarded as artifacts and are thus discarded.

$$\begin{aligned}
&\psi_1(n+1) = -\left\{\frac{\eta_{11}+\eta_{21}}{F_s} - 1\right\}\psi_1(n) + 2P_{e2}(n-n_2+1) + \\
&2\left\{\frac{\eta_{11}+\eta_{21}}{F_s} - 1\right\}P_{e2}(n-n_2) + P_{TM,1}(n+n_1+1) \quad - P_{TM,1}(n+ \\
&n_1) + \frac{\eta_{11}}{F_s}P_{TM,1}(n+n_1) + \frac{\eta_{21}}{F_s}P_{TM,1}(n-n_1) \\
&\psi_2(n+1) = -\left\{\frac{\eta_{12}+\eta_{22}}{F_s} - 1\right\}\psi_2(n) + P_{TM,2}(n+n_2+1) + \\
&P_{e2}(n+n_2+1) + P_{e2}(n-n_2+1) \quad + \left\{\frac{\eta_{12}}{F_s} - 1\right\}\{P_{TM,2}\,(n+ \\
&n_2) + P_{e2}(n+n_2) + P_{e2}(n-n_2)\} + \frac{\eta_{22}}{F_s}\{P_{TM,2}\,(n-n_2) + \\
&P_{e2}(n-n_2) + P_{e2}(n-3n_2)\}
\end{aligned} \tag{69}$$

Once the trans-mural pressures are reconstructed, the CV SYSID problem can be solved to identify the arterial dynamics by solving Equation (70). Since the trans-mural pressures are given as discrete-time sequences, Equation (64) is re-formulated in the time domain as follows. First, both the right-hand side and the left-hand side of Equation (64) are written into the discrete-time difference equations shown in Equation (69) (see the top of the page) via the forward difference approximation $s \cong F_s(z-1)$, where z is the discrete-time forward shift operator and F_s is the data sampling frequency. Second, for a given vector of unknowns Θ, the time series sequences of the new variables $\psi_1(n)$ and $\psi_2(n)$ are calculated by substituting $P_{TM,1}$, $P_{TM,2}$ and P_{e2} into Equation (69). Third, Θ is optimized so that the discrepancy between $\psi_1(n)$ and $\psi_2(n)$ is minimized:

$$\Theta^* = \arg\min_{\Theta \in D_\Theta} \|\psi_1(n,\Theta) - \psi_2(n,\Theta)\| \tag{70}$$

It is noted that the optimization in Equation (16) is not a trivial problem, because it involves the identification of both model structure and the model parameters. Indeed, the values of PTT $n_1 \triangleq [\tau_1 F_s]$ and $n_2 \triangleq [\tau_2 F_s]$ (where $[\cdot]$ returns the integer that is nearest to its argument) are not known a priori and must be identified together with the model parameters. Exploiting the fact that the arterial wave propagation dynamics are much more sensitive to the PTT than the remaining parameters [58], the SYSID problem formulated by Equation (70) is solved using a two-stage optimization problem: Equation (70) is solved multiple times over a physiologically relevant range of PTT (two-dimensional space spanned by τ_1 and τ_2), and the optimal set of parameters, Θ^*, is determined as the one with the smallest norm:

$$\Theta^* = \arg\min_{\tau_1,\tau_2}\left\{\min_{\eta_{ij}}\left\|\psi_1\left(n,\eta_{11}(\tau_1),\eta_{21}(\tau_1)\right) - \psi_2\left(n,\eta_{12}(\tau_2),\eta_{22}(\tau_2)\right)\right\|\right\} \quad (71)$$

subject to $\Theta \in D_\Theta$ and $i,j = 1,2$.

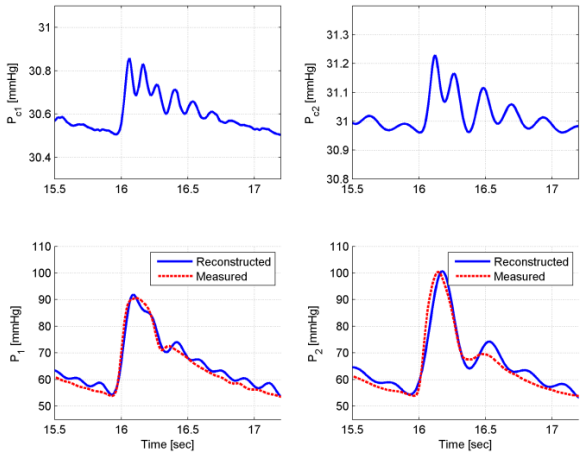

Figure 4-14 Measured versus Calibrated Peripheral ABPs

Figure 4-14 shows measured versus calibrated BP waveforms at the arm (left panels) and the leg (right panels) sensor sites, which illustrates that the empirical polynomial relationship in Equation (13) is effective in calibrating the cuff pressure oscillation to the arterial BP as well as to alleviate the nonlinear distortion induced by the BP cuff, once the frequency components in the cuff pressure oscillation responsible for arterial BP are properly separated from the harmonics due to the nonlinear artifacts of the BP cuff (which is discussed below; see also Figure 6).

Figure 4-15 depicts (i) the adverse impact of the nonlinearity in the BP cuff on the frequency spectrum of the arterial BP waveform and (ii) the effectiveness of the proposed approach to reject the artifact. The left two panels of Figure 4-15 indicates that the nonlinearity associated with the BP cuff introduces drastic distortions in the harmonic components, beyond 7 Hz and 4 Hz for P_{c1} and P_{c2}, respectively. The right two panels of Figure 4-15 compares the actual arterial BP with its reconstructed counterparts by (i) retaining the pre-specified number of harmonic components in the oscillation in P_{cj} (here, six and seven were used for arm and leg sites, respectively, as shown with the gold vertical lines) as proposed above and (ii) a brute-force low-pass filtering with 20 Hz cut-off frequency. It is obvious that fidelity of the reconstructed arterial BP can be significantly improved with the proposed than the brute-force approach. Although not shown, the alternative approach based on the fractional signal energy criterion resulted in arterial BP with comparable fidelity. It was observed that, on average over the eight subjects, retaining (i) six and seven harmonics for arm and

leg locations, or (ii) frequency contents corresponding to 90% and 95% of the total energy for arm and leg locations, respectively, yielded satisfactory performance in reconstructing the arterial BP from cuff pressure oscillations.

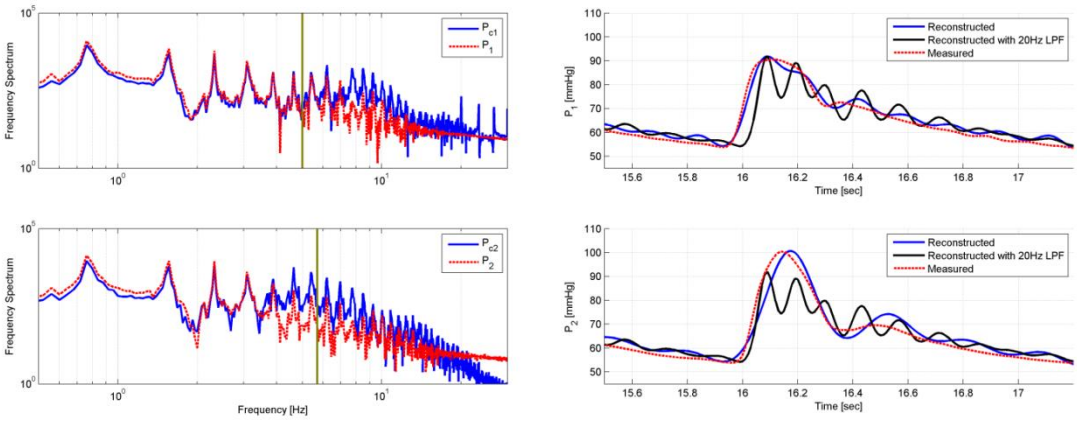

Figure 4-15 Rejection of Nonlinear Artifact of the Cuff and Reconstruction of ABP Waveforms

The actual versus reconstructed trans-mural pressures are shown in Figure 4-16 for arm (upper panel) and leg (lower panel) locations. Compared with the pure arterial BP in the absence of any active extra-vascular excitation pressures (see, for example, Figure 4-15), the active excitation contributed to create richer and more informative trans-mural pressure waves traveling in the arterial tree, which have potential to enhance the quality of CV SYSID significantly. The unique strength (and in fact a subtle challenge as well; see the Limitation of Study Section for details) of the proposed approach to reconstruct the trans-mural pressures is that it does not require a priori knowledge on the PTT τ_2 (which is not supposed to be available until SYSID is performed, unless additional measurements are provided) when separating the intra-vascular from the extra-vascular pressures.

Finally, the actual versus reconstructed central aortic BP waveforms are presented in Figure 8. The reconstructed central aortic BP was derived as follows (see Equation (69) for ψ_1 and ψ_2):

$$P_0^*(n) = \sigma_1\psi_1(n,\Theta^*) + \sigma_2\psi_2(n,\Theta^*) \tag{72}$$

where $\sigma_1 + \sigma_2 = 1$ (in this study, $\sigma_1 = \sigma_2 = \frac{1}{2}$ was used). It is obvious that the proposed active non-intrusive methodology for CV SYSID could successfully reconstruct the central aortic BP with fidelity (see Table 4-4 for the root-mean-squared waveform error (RMSE), errors in systolic and pulse pressures, and the r2 value), which supports its preliminary proof-of-principle and potential as a viable analytic option for CV hemodynamic monitoring.

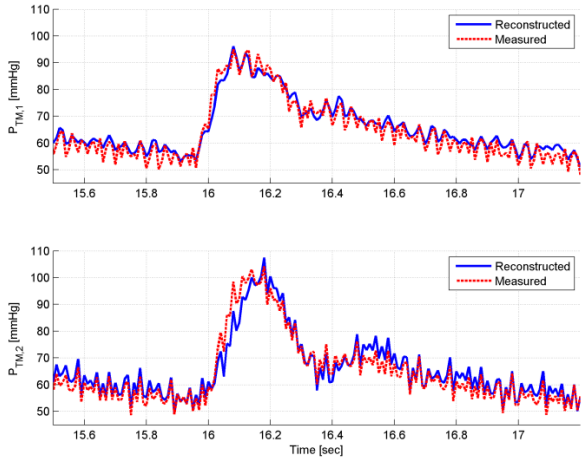

Figure 4-16 Actual versus reconstructed transmural pressure waveforms for CV SYSID

Finally, the active non-intrusive SYSID is compared with its passive counterpart and the direct peripheral BP (the radial BP was considered due to its routine availability in real clinical setting). Since the primary focus is the ability of the alternative approaches to estimate the central aortic BP, the comparison was made in terms of the errors associated with the accuracy of the central aortic BP waveform. Table 4-4 clearly shows that the proposed active SYSID outperforms the passive SYSID as well as the direct radial BP. For all the error metrics compared, the active SYSID resulted in smaller bias and tighter variance. The r2 value was also higher in the active than in the passive SYSID and the radial BP. Although the statistical significance was not established in this preliminary study due to the limited number of cases, Table 4-4 strongly assures the superiority of the active non-intrusive SYSID approach to its passive counterpart.

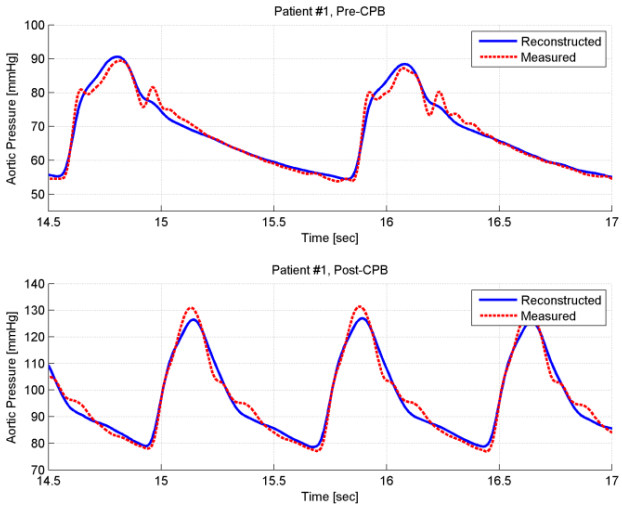

Figure 4-17 Actual versus reconstructed central aortic BP waveforms

Table 4-4 Comparison of active non-intrusive SYSID, passive non-intrusive SYSID and direct radial BP in estimating central aortic BP (mean±SD)

	RMSE [mmHg]	SP Error [mmHg]	PP Error [mmHg]	r^2 Value
Active SYSID	3.31±1.28	0.06±3.97	1.36±4.44	0.93±0.06
Passive SYSID	4.12±2.02	2.67±5.99	1.59±6.76	0.84±0.15
Radial BP	5.32±1.77	-8.55±10.77	-7.79±12.95	0.90±0.07

This study clearly demonstrated that the proposed active non-intrusive CV SYSID methodology has potential to result in enhanced CV SYSID outcomes than its passive counterpart (i.e. SYSID based upon the arterial BP alone) with richer and more informative transmural BP it can provide. Despite its overall success, this study has a few limitations.

First, the methodology was developed based upon a rather simplistic representation of the arterial tree: uniform lossless conduits connected in parallel to approximate upper- and lower-body circulations. In particular, this study neglected secondary wave reflections (called "re-reflections") known to occur in the arterial tree [29]. Further, this study implicitly assumed that the peripheral collocated actuation-sensing sites correspond to the terminal locations of the conduits, and that the actively excited extra-vascular pressure waves travel only to the heart, but not to further down the extremities. The validity of these simplifying assumptions must be investigated experimentally.

Second, in-depth study on the optimal active excitation is desired, in terms of both frequency range and amplitude of the excitation. Although the use of rather empirically selected band and amplitude of 20 Hz-35 Hz and 5 mmHg was efficacious in this study, we anticipate that the excitation of excessively high frequency range may not be effective due to the nonlinear and viscoelastic nature of the tissue mechanics, and also, too much increase in the amplitude of excitation may trigger the intrinsic CV control mechanism (the autonomic baroreceptor control). In this regard, more systematic understanding on the relationship between the active extra-vascular excitation and the resulting SYSID outcomes must be established.

Third, in separating the large-amplitude oscillation from its small-amplitude counterpart in P_{c2}, a critical assumption was made: that the large-amplitude oscillation corresponding to the active excitation is completely known by the input maneuver to the actuator (i.e. the open-loop input-output relationship of the actuator is known without uncertainty). This assumption may only be justified with the availability of highly accurate model of the actuator. In the future study, efforts to

improve the trans-mural pressure estimation and/or the SYSID procedure to relax the above rather restrictive assumption must be made.

In conclusion this chapter presented the development and the preliminary proof-of-principle of an innovative active non-intrusive SYSID methodology for CV monitoring. The methodology uses a dual collocated actuator-sensor system to actively excite the arterial tree and create rich and informative trans-mural pressure waves (actuation), and also to observe the trans-mural pressure waves non-intrusively (sensing). This study discussed algorithms to (i) estimate the trans-mural pressure waves and to (ii) identify the CV system dynamics based on the trans-mural pressure waves thus estimated. It was illustrated that the SYSID algorithm was able to accurately reconstruct the central aortic BP, and that its performance was superior to the passive non-intrusive approach with statistical significance. It is anticipated that the proposed active non-intrusive SYSID paradigm will enhance our ability to monitor CV health and diagnose CVD.

Chapter 5 – Conclusions and Future Directions

5.1: Conclusions and Summary

This thesis aimed to introduce a noninvasive cardiovascular health monitoring methodology employing blood pressure cuffs and demonstrate its feasibility. In order to accomplish this goal:

- In chapter two the tube-load model was introduced and described mathematically in its single and double tube manifestations. It was experimentally demonstrated that the tube-load model is capable of describing accurately and reliably the relationship between central and peripheral blood pressures in humans using invasively recorded data from humans undergoing surgery. The tube-load model serves as the foundation for health monitoring techniques described in this thesis and its validation in humans is of the utmost importance. Prior to this study the authors have no knowledge of an extensive quantative validation of the tube-load model in humans so as a first step toward the development of successful health monitoring techniques this step was deemed important.
- In chapter three the individualized transfer function (ITF) methodology was presented and mathematically described. The ITF methodology uses two diametrically opposed peripheral blood pressure waveforms to estimate the central aortic blood pressure waveform. Many studies indicate that the central aortic blood pressure waveform plays an important part in evaluating cardiovascular health and that peripheral arterial blood pressures are not adequate replacements. In order to validate the ITF methodology invasively recorded data measured at the central aortic, radial and femoral arteries was utilized and a commonality of the pressure waveforms measured at the peripheries (i.e. the radial and femoral blood pressures) was exploited to reproduce an estimate of central aortic blood pressure using the tube-load model validated in chapter 2. This thesis demonstrated that central aortic blood pressure could accurately, reliably and robustly be estimated in a diverse set of hemodynamic conditions and that the estimate outperformed the estimation made by the peripheral blood pressures used as surrogates to the central aortic blood pressure.
- In chapter four an active noninvasive individualized transfer function was introduced and described mathematically. The purpose of this newly proposed methodology is to overcome some of the inherent limitations of the ITF methodology, i.e. the invasive nature of the measurements of the peripheral blood pressures and also the lack of frequency richness in the central aortic blood pressure produced by the heart. The proposed methodology utilized a

dual blood pressure cuff system to simultaneously noninvasively measure peripheral blood pressures and actuate the arterial tree to create rich transmural blood pressures to improve the quality of the signals for the purposes of system identification. It was demonstrated in this feasibility study that this methodology is capable of outperforming the passive noninvasive counterpart in estimating central aortic BP and radial blood pressure as a surrogate to central BP.

5.2: Anticipated Benefits and Contributions

It is anticipated that the findings of this thesis will be foundations for developing further cardiovascular health monitoring techniques. The ITF methodology can be utilized in certain operations or conditions to continuously monitor the central aortic blood pressure and assist in diagnosis of cardiovascular disease based not only on systolic and diastolic blood pressures but also making use of waveform morphology.

The active noninvasive system identification methodology can potentially be developed into a commercial device easily used in common medical services centers and also possibly at home. This methodology encompasses several key necessities of all technologies that want to make their way into the modern commercial devices age, i.e. that they must be relatively cheap, noninvasive and easily usable. The active noninvasive methodology utilizes blood pressure cuffs which are familiar to patients and also cheap and the mathematics can be encoded onto a microchip, making it easily accessible and easy to use for users.

The multichannel blind system identification approach applied to the tube-load model can further be exploited and applied to other systems with multiple measurable and distinct end-points, for just 1 example one can consider the diabetes problem where phosphor and glucose levels can be measured independently and the multichannel blind system identification methodology can be applied to estimate the amount of insulin in the plasma of the subject.

5.3: Future Directions

In this study a preliminary methodology for noninvasive active system identification of the arterial tree was introduced and it was demonstrated that the methodology can estimate the central aortic blood pressure accurately. It is anticipated that to build on this preliminary study the following steps can be taken to realize a fully experimental study to further validate the feasibility of the outlined methodology:

1. Validation of the external excitation wave propagation phenomena:

   In this study the external excitation provided to the arterial tree through the collocated actuator sensor system is assumed to propagate through the tube that it is applied in a lossless manner. In future studies building on this work externally applied excitations should be tested in practice to demonstrate the propagation of the excitations through the arterial tree. One possible way is to apply two thigh cuffs or a thigh and arm cuff, apply an external excitation at one thigh cuff and pick-up the resulting propagated external excitations in the opposing cuff. Other possibilities include performing the same maneuver with the cuff and pick-up the oscillations utilizing a tonometer. This step is important due to the propagation of the externally produced excitations being a key component to producing rich transmural blood pressures to produce accurate and reliable estimates of the parameters characterizing the arterial tree. It is noted that in this thesis the data utilized for the feasibility study was an amalgamation on invasively measured data and artificially produced data.

2. Validation of the noninvasive blood pressure measurements:

   In this study the peripheral blood pressures are estimated through a protocol outlined in chapter 4. The feasibility of this protocol was demonstrated utilizing a complex and previously validated model of the cuff, tissue and hemodynamics model. Further experimental validation of this protocol is required to prove the feasibility of the active noninvasive system identification methodology. Possible methodologies for the validation of the noninvasive blood pressure protocol can be to simultaneously measure arterial blood pressure and cuff oscillations at the same location and validate viscoelastic models or to measure cuff oscillations at the brachial artery and utilizing a viscoelastic model of the artery, tissue and cuff along with a tube-load model, relate this measured cuff oscillation signal to a blood pressure signal measured at the finger location.

3. Fully experimental validation of the active noninvasive system identification methodology:

   In order to fully realize the active noninvasive system identification methodology experimentally the collocated actuator and sensor system needs to be attached to a subject and invasive measurements of the central aortic blood pressure along with the rich transmural blood pressures created by the actuator need to be recorded simultaneously. Once the protocol is implemented and an estimate of the central aortic blood pressure is created, it

will be compared to the measured counterpart to evaluate its accuracy this will serve as a criteria in order to evaluate the effectiveness of the active noninvasive system identification methodology. The active methodology can be compared to a passive counterpart by removing the excitation and utilizing the criteria in order to ensure a more accurate estimation can be made by the active methodology. Finally if peripheral passive invasive signals are available previously developed ITF methodology can be utilized to estimate central aortic blood pressure and compare this methodology with the active noninvasive methodology to evaluate which is more accurate.

4. Extension of the arterial tree model to account for losses in the arterial tree

   In the active noninvasive methodology developed in this thesis, the arterial tree was modeled by an asymmetric 2 tube-load model and the tube-load models were assumed to be lossless. It has previously been demonstrated that the tube-load model in its lossless form is an accurate and reliable model estimating the wave propagation and hemodynamics of the human arterial tree [59]. Investigating the effects of incorporating losses in the tube-load model and its potential impact on the performance of the active noninvasive methodology would be of importance for further developing a model based understanding of the wave propagation and hemodynamics.

Bibliography

[1] V. L. Roger, A. S. Go, D. M. Lloyd-Jones, R. J. Adams, J. D. Berry, T. M. Brown, *et al.*, "Heart disease and stroke statistics--2011 update: a report from the American Heart Association," *Circulation,* vol. 123, pp. e18-e209, 2011.

[2] W. S. Weintraub, S. R. Daniels, L. E. Burke, B. A. Franklin, D. C. Goff, L. L. Hayman, *et al.*, "Value of Primordial and Primary Prevention for Cardiovascular Disease: A Policy Statement From the American Heart Association," *Circulation,* vol. 124, 2011.

[3] V. L. Roger, A. S. Go, L.-J. D.M., E. J. Benjamin, J. D. Berry, W. B. Borden, *et al.*, "Heart disease and stroke statistics--2012 update: a report from the American Heart Association," *Circulation,* vol. 125, pp. e2-e220, 2012.

[4] J. Stokes, W. B. Kannel, P. A. Wolf, R. B. D'Agostino, and L. A. Cupples, "Blood pressure as a risk factor for cardiovascular disease the Framingham Study--30 years of follow-up," *Hypertension,* vol. 13, pp. I13-I18, 1989.

[5] W. W. Nichols and M. F. O'Rourke, *Mcdonald's Blood Flow in Arteries*. New York: Oxford University Press, Inc., 1998.

[6] A. P. Avolio, L. M. Van Bortel, P. Boutouyrie, J. R. Cockcroft, C. M. McEniery, A. D. Protogerou, *et al.*, "Role of pulse pressure amplification in arterial hypertension experts' opinion and review of the data," *Hypertension,* vol. 54, pp. 375-383, 2009.

[7] C. Vlachopoulos, K. Aznaouridis, and C. Stefanadis, "Prediction of cardiovascular events and all-cause mortality with arterial stiffness: a systematic review and meta-analysis," *Journal of American College of Cardiology,* vol. 55, pp. 1318-1327, 2010.

[8] W. W. Nichols, "Clinical measurement of arterial stiffness obtained from noninvasive pressure waveforms," *American Journal of Hypertension,* vol. 18, pp. 3S-10S, 2005.

[9] W. W. Nichols, S. J. Denardo, I. B. Wilkinson, C. M. McEniery, J. Cockcroft, and M. F. O'Rourke, "Effects of arterial stiffness, pulse wave velocity, and wave reflections on the central aortic pressure waveform," *Journal of Clinical Hypertension (Greenwich),* vol. 10, pp. 295-303, 2008.

[10] M. E. Safar, J. Blacher, B. Pannier, A. P. Guerin, S. J. Marchais, P. M. Guyonvarc'h, *et al.*, "Central pulse pressure and mortality in end-stage renal disease," *Hypertension,* vol. 39, pp. 735-738, 2002.

[11] R. Pini, M. C. Cavallini, V. Palmieri, N. Marchionni, M. Di Bari, R. B. Devereux, *et al.*, "Central but not brachial blood pressure predicts cardiovascular events in an unselected geriatric population: the ICARe Dicomano Study," *Journal of American College of Cardiology,* vol. 51, pp. 2432-2439, 2008.

[12] P. Jankowski, K. Kawecka-Jaszcz, D. Czarnecka, M. Brzozowska-Kiszka, K. Styczkiewicz, M. Loster, *et al.*, "Pulsatile but not steady component of blood pressure predicts cardiovascular events in coronary patients," *Hypertension,* vol. 51, pp. 848-855, 2008.

[13] M. E. Safar and P. Jankowski, "Central blood pressure and hypertension: role in cardiovascular risk assessment," *Clinical Science,* vol. 116, pp. 273-282, 2009.

[14] O. Vardoulis, T. G. Papaioannou, and N. Stergiopulos, "On the estimation of total arterial compliance from aortic pulse wave velocity," *Annals of Biomedical Engineering*, vol. 40, pp. 2619-2626, 2012.
[15] Yasmin and M. J. Brown, "Similarities and differences between augmentation index and pulse wave velocity in the assessment of arterial stiffness," *Quarterly Journal of Medicine*, vol. 92, pp. 595-600, 1999.
[16] I. B. Wilkinson, S. A. Fuchs, I. M. Jansen, J. C. Spratt, G. D. Murray, J. R. Cockcroft, *et al.*, "Reproducibility of pulse wave velocity and augmentation index measured by pulse wave analysis," *Journal of Hypertension*, vol. 16, pp. 2079-2084, 1998.
[17] B. E. Westerhof, I. Guelen, N. Westerhof, J. M. Karemaker, and A. Avolio, "Quantification of wave reflection in the human aorta from pressure alone a proof of principle," *Hypertension*, vol. 48, pp. 595-601, 2006.
[18] J. G. Kips, E. R. Rietzschel, M. L. De Buyzere, B. E. Westerhof, T. C. Gillebert, L. M. Van Bortel, *et al.*, "Evaluation of noninvasive methods to assess wave reflection and pulse transit time from the pressure waveform alone," *Hypertension*, vol. 53, pp. 142-149, 2009.
[19] A. Qasem and A. Avolio, "Determination of aortic pulse wave velocity from waveform decomposition of the central aortic pressure pulse," *Hypertension*, vol. 51, pp. 1-8, 2008.
[20] C. H. Chen, E. Nevo, B. Fetics, P. H. Pak, F. C. Yin, W. L. Maughan, *et al.*, "Estimation of central aortic pressure waveform by mathematical transformation of radial tonometry pressure. Validation of generalized transfer function," *Circulation*, vol. 95, pp. 1827-1836, 1997.
[21] E. Kroeker and E. Wood, "Comparison of simultaneously recorded central and peripheral arterial pressure pulses during rest, exercise, and tilted position in man," *Circulation Research*, vol. 3, pp. 623-632, 1955.
[22] M. Karamanoglu, M. F. O'Rourke, A. P. Avolio, and R. P. Kelly, "An analysis of the relationship between central aortic and peripheral upper limb pressure waves in man," *European Heart Journal*, vol. 14, pp. 160-167, 1993.
[23] E. Agabiti-Rosei, G. Mancia, M. F. O'Rourke, M. J. Roman, M. E. Safar, H. Smulyan, *et al.*, "Central blood pressure measurements and antihypertensive therapy a consensus document," *Hypertension*, vol. 50, pp. 154-160, 2007.
[24] K. Sagawa, R. K. Lie, and J. Schaefer, "Translation of Otto frank's paper "Die Grundform des arteriellen Pulses" zeitschrift für biologie 37: 483–526 (1899)," *Journal of Molecular and Cellular Cardiology*, vol. 22, pp. 253-254, 1990.
[25] J. O. Hahn, A. T. Reisner, and H. H. Asada, "Blind identification of 2-channel IIR systems with application to central cardiovascular monitoring," *ASME Journal of Dynamic Systems, Measurement and Control*, vol. 131, p. 051009, 2009.
[26] G. Zhang, J. O. Hahn, and R. Mukkamala, "Tube-load model parameter estimation for monitoring of arterial hemodynamics," *Frontiers in Computational Physiology and Medicine*, vol. 2, pp. 1-18, 2011.
[27] K. L. Wang, H. M. Cheng, S. H. Sung, S. Y. Chuang, C. H. Li, H. A. Spurgeon, *et al.*, "Wave reflection and arterial stiffness in the prediction of 15-year all-cause and cardiovascular mortalities a community-based study," *Hypertension*, vol. 55, pp. 799-805, 2010.

[28] R. Burattini and K. B. Campbell, "Modified asymmetric T-tube model to infer arterial wave reflection at the aortic root," *IEEE Transactions on Biomedical Engineering*, vol. 36, pp. 805-814, 1989.
[29] K. B. Campbell, R. Burattini, D. L. Bell, R. D. Kirkpatrick, and G. G. Knowlen, "Time-domain formulation of asymmetric T-tube model of arterial system," *American Journal of Physiology*, vol. 258, pp. H1761-H1774, 1990.
[30] W. Welkowitz, Q. I. N. G. Cui, Y. Qi, and J. B. Kostis, "Noninvasive estimation of cardiac output," *IEEE Transactions on Biomedical Engineering*, vol. 38, pp. 1100-1105, 1991.
[31] D. S. Berger, J. K.-J. Li, W. K. Laskey, and A. Noordergraff, "Repeated reflection of waves in the systemic arterial system," *American Journal of Physiology*, vol. 264, pp. H269-H281, 1993.
[32] S. G. Shroff, D. S. Berger, C. Korcarz, R. M. Lang, R. H. Marcus, and D. E. Miller, "Physiological relevance of T-tube model parameters with emphasis on arterial compliance," *American Journal of Physiology*, vol. 269, pp. H365-H374, 1995.
[33] R. Fogliardi, R. Burattini, and K. B. Campbell, "Identification and physiological relevance of an exponentially tapered tube model of canine descending aortic circulation," *Medical Engineering and Physics*, vol. 19, pp. 201-211, 1997.
[34] P. Segers, S. Carlier, A. Pasquet, S. I. Rabben, L. R. Hellevik, E. Remme, *et al.*, "Individualizing the aorto-radial pressure transfer function: feasibility of a model-based approach," *American Journal of Physiology*, vol. 279, pp. H542-H549, 2000.
[35] M. R. and D. Xu, "Continuous and less invasive central hemodynamic monitoring by blood pressure waveform analysis," *American Journal of Physiology*, vol. 299, pp. H584-H599, 2010.
[36] G. Swamy, Q. Ling, T. Li, and R. Mukkamala, "Blind identification of the aortic pressure waveform from multiple peripheral artery pressure waveforms," *American Journal of Physiology*, vol. 292, pp. H2257-H2264, 2007.
[37] M. R. El-Tahan, "Preoperative ephedrine counters hypotension with propofol anesthesia during valve surgery: a dose dependent study," *Annals of Cardiac Anesthesia*, vol. 14, pp. 30-40, 2011.
[38] J. O. Hahn, A. T. Reisner, H. H. Asada, and F. A. Jaffer, "Subject-specific estimation of central aortic blood pressure using an individualized transfer function: a preliminary feasibility study," *IEEE Journal of Biomedical and Health Informatics*, vol. 16, pp. 212-220, 2012.
[39] J. O. Hahn, A. T. Reisner, and H. H. Asada, "Estimation of pulse transit time using two diametric blood pressure waveform measurements," *Medical Engineering and Physics*, vol. 32, pp. 753-759, 2010.
[40] C. U. Choi, E. J. Kim, S. H. Kim, S. Y. Shin, U. J. Choi, J. W. Kim, *et al.*, "Differing effects of aging on central and peripheral blood pressures and pulse wave velocity: a direct intraarterial study," *Journal of Hypertension*, vol. 28, pp. 1252-1260, 2010.
[41] T. K. Waddell, A. M. Dart, T. L. Medley, J. D. Cameron, and B. A. Kingwell, "Carotid pressure is a better predictor of coronary artery disease severity than brachial pressure," *Hypertension*, vol. 38, pp. 927-931, 2001.

[42] G. Swamy, D. Xu, N. B. Olivier, and R. Mukkamala, "An adaptive transfer function for deriving the aortic pressure waveform from a peripheral artery pressure waveform," *American Journal of Physiology*, vol. 297, pp. H1956-H1963, 2009.
[43] L. Ljung, *System Identification: Theory for the User*. Upper Saddle River, NJ: Prentice-Hall, 1999.
[44] W. J. Stok, B. E. Westerhof, and J. M. Karemaker, "Changes in finger-aorta pressure transfer function during and after exercise," *Journal of Applied Physiology*, vol. 101, pp. 1207-1214, 2006.
[45] M. Sugimachi, T. Shishido, K. Miyatake, and K. Sunagawa, "A new model-based method of reconstructing central aortic pressure from peripheral arterial pressure," *Japanese Journal of Physiology*, vol. 51, pp. 217-222, 2001.
[46] N. Fazeli, C. S. Kim, and J. O. Hahn, "Non-invasive estimation of central blood pressure waveform using a dual diametric cuff system: a preliminary study," in *Annual ASME-FDA Frontiers in Medical Devices Conference*, Washington, DC, USA, 2013.
[47] S. Wassertheurer, J. Kropf, T. Weber, M. Van der Giet, J. Baulmann, M. Ammer, *et al.*, "A new oscillometric method for pulse wave analysis: comparison with a common tonometric method " *Journal of Human Hypertension*, vol. 24, pp. 498-504, 2010.
[48] A. C. W. Lin, A. Lowe, K. Sidhu, W. Harrison, P. Ruygrok, and R. Stewart, "Evaluation of a novel sphygmomanometer, which estimates central aortic blood pressure from analysis of brachial artery suprasystolic pressure waves," *Journal of Hypertension*, vol. 30, pp. 1743-1750, 2012.
[49] A. T. Reisner, P. A. Shaltis, D. B. McCombie, and H. H. Asada, "Utility of the photoplethysmogram in circulatory monitoring," *Anesthesiology*, vol. 108, pp. 950-958, 2008.
[50] Y.-T. Shih, H.-M. Cheng, S.-H. Sung, W.-C. Hu, and C.-H. Chen, "Comparison of two generalized transfer functions for measuring central systolic blood pressure by an oscillometric blood pressure monitor," *Journal of Human Hypertension*, vol. 27, pp. 204-210, 2013.
[51] A. Figueroa, "Effects of resistance training on central blood pressure and wave reflection in obese adults with prehypertension," *Journal of Human Hypertension*, vol. 28, pp. 143-144, 2013.
[52] F. C. STARMER, P. A. MCHALE, F. R. COBB , and J. GREENFIELD, "Evaluation of Several Methods for Computing Stroke Volume from Central Aortic Pressure," *Circulation Research*, vol. 33, pp. 139-148, 1973.
[53] C. S. Kim, N. Fazeli, M. S. McMurtry, B. A. Finegan, and J. O. Hahn, "Quantification of Wave Reflection Using Peripheral Blood Pressure Waveforms," *IEEE Journal of Biomedical and Health Informatics*, 2014.
[54] J. A. Kong, *Eletromagnetic Wave Theory*: EMW Publishing, 2008.
[55] M. Ursino and C. Cristalli, "A mathematical study of some biomechanical factors affecting the oscillometric blood pressure measurement," *IEEE Transactions on Biomedical Engineering*, vol. 43, pp. 761-778, 1996.
[56] S. Wassertheuer, J. Kropf, T. Weber, M. van der Giet, J. Baulmann, M. Ammer, *et al.*, "A new oscillometric method for pulse wave analysis: comparison

with a common tonometric method," *Journal of Human Hypertension*, vol. 24, pp. 498-504, 2010.
[57] M. Stork and J. Jilek, "Cuff pressure pulse waveforms: their current and prospective applications in biomedical instrumentation," in *Biomedical Engineering, Trends in Electronics, Communications and Software*, A. N. Laskovski, Ed., ed: InTech, 2011, pp. 193-210.
[58] B. P. Imholz, M. W. Wieling, G. A. van Montfrans, and K. H. Wesseling, "Fifteen years experience with finger arterial pressure monitoring: assessment of the technology," *Cardiovascular Research*, vol. 38, 1998.
[59] N. Fazeli, M. Rashedi, A. Chappell, S. Wang, R. MacArthur, M. S. McMurtry, B. A. Finegan, and J. O. Hahn, "Subject-Specific Estimation of Aortic Blood Pressure via System Identification: Preliminary In-Human Experimental Study," in *American Control Conference*, 2013.
[60] N. Fazeli and J. O. Hahn, "Active non-intrusive system identification for cardiovascular monitoring Part II: System identification algorithm development," in *ASME Dynamic Systems and Control Conference*, 2013.
[61] N. Fazeli, H. C. Kim, and J. O. Hahn, "Active non-intrusive system identification for cardiovascular monitoring Part I: Excitation and measurement protocol design," in *ASME Dynamic Systems and Control Conference*, 2012, pp. DSCC2012–8579.
[62] M. Rashedi, N. Fazeli, A. Chappell, S. Wang, R. MacArthur, M. S. McMurtry, B. A. Finegan, and J. O. Hahn, "Modeling and system identification of arterial hemodynamics in humans," in *Dynamic Systems and Control Conference*, 2013.